Science of the Total Environment 898 (2023) 166397

Contents lists available at ScienceDirect

Science of the Total Environment

journal homepage: www.elsevier.com/locate/scitotenv

Mapping potentially groundwater-dependent vegetation in the Mediterranean biome using global geodata targeting site conditions and vegetation characteristics

Léonard El-Hokayem [a,b,*], Pantaleone De Vita [c], Muhammad Usman [a], Andreas Link [d], Christopher Conrad [a,b]

[a] Institute of Geosciences and Geography, Martin Luther University Halle-Wittenberg, Halle (Saale) 06120, Germany
[b] German Centre for Integrative Biodiversity Research (iDiv) Halle-Jena-Leipzig, Leipzig 04103, Germany
[c] Department of Earth, Environmental and Resources Sciences, University of Naples Federico II, Naples 80126, Italy
[d] Chair of Sustainable Engineering, Technical University of Berlin, Berlin 10623, Germany

HIGHLIGHTS

- Potentially groundwater-dependent vegetation (pGDV) was derived for the Mediterranean biome.
- The novel pGDV index integrates globally-available remote sensing and geodata.
- Vegetation surveys and regional pGDV maps show moderate to good agreement with the pGDV index.
- 31 % of the naturally vegetated areas in the Mediterranean likely depend on groundwater.
- The pGDV index supports the local identification of actual GDV and biodiversity conservation.

GRAPHICAL ABSTRACT

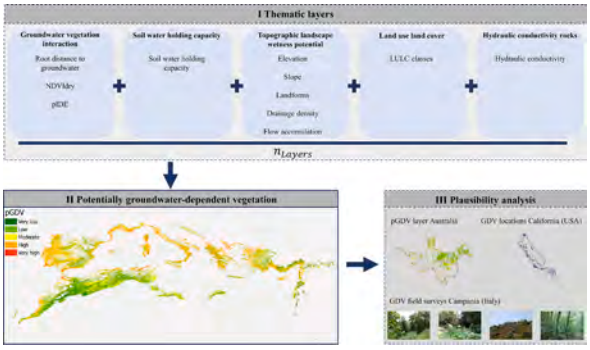

ARTICLE INFO

Editor: Christian Herrera

Keywords:
Groundwater-dependent vegetation
Remote sensing
Mediterranean
Geodata integration
Biodiversity hotspots

ABSTRACT

Groundwater-dependent vegetation (GDV) is essential for maintaining ecosystem functions and services, providing critical habitat for species, and sustaining human livelihoods. However, climate and land-use change are threatening GDV, highlighting the need for harmonised, global mapping of the distribution and extent of GDV. This need is particularly crucial in vulnerable biodiversity hotspots such as the Mediterranean biome. This study presents a novel multicriteria index to identify areas in the Mediterranean biome that provide suitable environmental conditions to support potentially groundwater-dependent vegetation (pGDV) where vegetation behaviour is also indicative of groundwater use. Global datasets targeting 1) groundwater vegetation interaction; 2) soil water holding capacity; 3) topographical landscape wetness potential; 4) land use land cover and 5) hydraulic conductivity of rocks have been combined for the first time in an easy-to-use index. Layer weightings from Analytical Hierarchy Process and Random Forest showed limited applicability on biome scale, but an unweighted overlay of eleven thematic layers produced plausible results. The final pGDV map indicates that 31 % of the natural vegetation in the Mediterranean biome likely depend on groundwater. Moreover, moderate to

* Corresponding author at: Institute of Geosciences and Geography, Martin Luther University Halle-Wittenberg, Halle, Saale 06120, Germany.
E-mail address: leonard.el-hokayem@geo.uni-halle.de (L. El-Hokayem).

https://doi.org/10.1016/j.scitotenv.2023.166397
Received 19 May 2023; Received in revised form 25 July 2023; Accepted 15 August 2023
Available online 19 August 2023

good agreement was found compared to actual GDV locations in Campania, Italy (91 % with at least moderate potential) and California, USA (87 % with at least moderate potential). The results provide valuable information for identifying regions with a substantial presence of pGDV in the Mediterranean biome and can be used for decision making, e.g. to prioritise field surveys and high-resolution remote sensing for GDV mapping. It can therefore support effective groundwater resource management and the conservation of biodiversity hotspots.

1. Introduction

In the Mediterranean biome, known for its high plant diversity (Mittermeier et al., 2005), 50 % of the plants use groundwater (Evaristo and McDonnell, 2017), at least in the dry periods of the year (Barbeta et al., 2015). However, a decline in winter precipitation and increased groundwater use for consumption and irrigation exacerbate water stress in this biome, threatening vegetation and ultimately biodiversity (Pérez Hoyos et al., 2016; Tuel and Eltahir, 2020; Underwood et al., 2009). In this context, the identification of groundwater-dependent vegetation (GDV) can be assessed as an initial step of paramount relevance for ensuring the conservation of endangered ecosystem services (Kløve et al., 2014; Pérez Hoyos et al., 2016).

Several ground-based methods, including phreatophyte (Meinzer, 1927) and habitat mapping (Killroy et al., 2008), or stable isotope analyses (Jones et al., 2020) allow for direct identification of GDV, which however is resource intensive and hence limited to local scale application (Pérez Hoyos et al., 2016). At larger scales, remote sensing (RS) and geodata integration gained importance in the identification of GDV, although these datasets indicate potential locations of GDV instead of actual occurrences (hereafter referred to as potentially groundwater-dependent vegetation (pGDV)).

Different thematic layers and datasets have been explored for the identification of pGDV. Common criteria include, the delineation of green islands (Akasheh et al., 2008) together with analyses of topographically driven water availability (Münch and Conrad, 2007) from RS. For instance, Páscoa et al. (2020) mapped pGDV in the Iberian Peninsula (IP) based on MODIS Normalized Difference Vegetation Index (NDVI) timeseries. Liu et al. (2021) used MODIS data to map pGDV in Central Asia, targeting vegetation that remains green during the summer dry period and shows low seasonal and interannual changes in vitality. Similar approaches have been used to map potentially groundwater-dependent ecosystems (pGDEs), which also include wetlands, rivers or springs (Eamus et al., 2006). Recently, in addition to vegetation characteristics, environmental site conditions have gained attention in the detection of pGDE. Martínez-Santos et al. (2022) included permeability, geology, soil, groundwater table depth (GWTD), NDVI, topographic wetness index (TWI), slope and flow accumulation in a supervised classification to identify wetlands in Spain. Doody et al. (2017) focused on system recharge, groundwater availability, soil, lithology and vegetation types as well as RS-based identification of wet areas in a weighted index to map pGDEs in Australia.

Data integration is also an essential feature in the mapping of groundwater potential zones (GWPZ), e.g. for the detection of exploitable groundwater resources (Arulbalaji et al., 2019; Pande et al., 2021). The GWPZ approach resembles the research on pGDE mapping, as several environmental parameters are combined that hint at the presence of groundwater, e.g., through multi-criteria decision analysis, weighted-overlay, or machine learning (Arulbalaji et al., 2019; Martínez-Santos and Renard, 2020; Pande et al., 2021). Recently, Duran-Llacer et al. (2022) proposed a method that combines GWPZ-mapping with multispectral indices to map zones that likely contain pGDEs in semi-arid environments. Nevertheless, transferability to other regions, as well as application at the biome level depends on the availability of input data or appropriate weighting and has not been tested yet.

From a mapping perspective, one challenge is the range of scales and resolutions in the geodata applied for these approaches, as globally applicable data are mixed with local ground data (e.g., Doody et al., 2017; Duran-Llacer et al., 2022). Also, the detection of pGDV over extensive areas remains difficult, because supporting data with sufficiently high resolution are rare (Glanville et al., 2023). For instance, whilst high-resolution RS data for detecting pGDV (e.g., Doody et al., 2017; El-Hokayem et al., 2023; Gou et al., 2015) is available at the global scale, required and detailed hydrogeological or edaphic information is mainly available at local scale only. Using high-resolution RS data globally challenges also in terms of computation intensity and storage demands.

However, in face of these trade-offs, and with the exception of Link et al. (2023) who mapped global pGDEs at 0.5° spatial resolution, pGDV maps are available from local to continental scale only. There are no maps available that cover the entire Mediterranean biome at global scale.

In this study, we present a novel approach to detect areas in the Mediterranean biome providing suitable conditions to hold pGDV where vegetation behaviour also indicates groundwater use, at least in the dry period (partially dependent on groundwater). Therefore, global data is combined with a simple index. The index aims to identify areas where high groundwater potential exists and groundwater is also likely to be accessible for plants. GWPZ-mapping parameters are complemented with vegetation-related RS parameters to address: 1) groundwater vegetation interaction (GVI); 2) soil water holding capacity (SWHC); 3) topographic landscape wetness potential (TLWP); 4) land use land cover (LULC) and 5) hydraulic conductivity of rocks (K) in an easy-to-use index showing low to high pGDV. Input data is globally and openly available. Expert-based and automated methods are compared to find the optimal approach for combining the parameters. The plausibility of the pGDV map is tested against GDV layers in Australia (Doody et al., 2017) and California (USA) (Klausmeyer et al., 2018) and ground truth vegetation data in Campania (Italy).

To identify pGDV, we combine, for the first time, several global datasets into a harmonised index. Such a novel index should allow the identification of regions with a high proportion of pGDV in the Mediterranean biome, but is ideally transferable to other semi-arid environments. The potential utility of the index is to decide where high-resolution mapping of actual GDV could be applied, e.g. to ensure sustainable groundwater management and to protect GDV as local biodiversity hotspots.

2. Material and methods

To calculate the pGDV index we integrated thematic layers focussing on GVI, SWHC, TLWP, LULC and K (Fig. 1). We tested layer weighting via an expert-based approach through Analytical Hierarchy Process (AHP) as well as using Random Forest (RF). Existing pGDV calculated for Australia (Doody et al., 2017), ground truth vegetation data for Campania (El-Hokayem et al., 2023, and new field samplings), as well as GDV locations in California (Klausmeyer et al., 2018), are used to analyse the plausibility of the produced Mediterranean pGDV map.

2.1. Study extent

The zonal vegetation of the five Mediterranean regions consists of subtropical evergreen and broadleaved forests and shrublands dominated by sclerophyllous woody plants. Despite differences in species composition and structure between holm oak forests and maquis of the Mediterranean Basin, the South African fynbos, the Californian

chaparral, the matorral of central Chile and the karri forests of Australia, physiognomic similarities exist (Pignatti, 2003). Mean annual temperatures in the Mediterranean climate range between 14 °C and 18 °C. The annual rainfall varies between 400 mm and 1200 mm and is characterised by wet winters (at least 65 % of the annual rainfall) and summer droughts leading to a severe soil water deficit in summer. During this period, the plants are exposed to severe stress that lasts for 3–5 months (Pignatti, 2003). Within the Mediterranean biome, temperate climates with a dry and hot summer (Csa) and arid, cold steppes (BSk) dominate (Beck et al., 2018). Climates without an annual dry season (Beck et al., 2018) were excluded from our analysis. Fig. 2 presents an overview of the Mediterranean biome and the calculated beginning of the annual 16 weeks dry period per basin as week of the year.

2.2. Thematic layer selection

To detect pGDV, we integrated thematic layers and methods widely used in the delineation of GWPZ (e.g., Arulbalaji et al., 2019; Mohan et al., 2018; Singh et al., 2013) and pGDEs (Doody et al., 2017; Duran-Llacer et al., 2022; Gomes Marques et al., 2019; Páscoa et al., 2020). The index aims to identify landscapes where high groundwater potential exists and groundwater is also likely to be accessible for plants. Thus, environmental site conditions would allow for the presence of pGDV. We included eight out of the ten most used parameters in GWPZ studies (Thanh et al., 2022). Topographic wetness index (TWI) and lineament density were excluded due to limited global applicability. However, flow accumulation is used alternatively to TWI. Additional input parameters targeting GVI (e.g., Doody et al., 2017; Duran-Llacer et al., 2022) such as vitality or distance to groundwater were integrated. Five major parameters (GVI, SWHC, TLWP, LULC, K) consisting of eleven thematic layers are aggregated in a pGDV index on the biome level. Thematic layers either determine pGDV occurrence through favourable site conditions (RDGW, SWHC, TLWP) or control pGDV detection (pIDE, $NDVI_{dry}$, LULC). CPU-intensive processing steps and data acquisition were performed in Google Earth Engine (GEE) (Gorelick et al., 2017).

Thematic layers and datasets used in the index composition are listed in Table 1 and described in the following subchapters. Time series data for evapotranspiration, precipitation and NDVI were extracted for the period 2003–2021 and mean values were calculated over this period. All other datasets, however, mark a fixed point in time.

2.2.1. Groundwater vegetation interaction (GVI)

Besides parameters that define groundwater potential in terms of groundwater storage (Rodell et al., 2007), yield (Nampak et al., 2014), or quality (Dhar et al., 2015), the interaction between groundwater and vegetation must be characterised to map pGDV. The most limiting parameter for the growth and survival of GDV is root access to groundwater resources (Doody et al., 2017; Gomes Marques et al., 2019). Other studies on GDV further focus on areas that maintain greenness constant during dry periods, between seasons and interannually (e.g., Liu et al., 2021; Gou et al., 2015; Páscoa et al., 2020). ET rates exceeding precipitation further indicate external water inflows to the ecosystem, such as groundwater (Doody et al., 2017).

2.2.1.1. Root distance to groundwater (RDGW). To estimate whether roots may access groundwater resources, we combined three global datasets related to hydrogeology (GWTD), soil texture and vegetation (rooting depth) (Link et al., 2023). Globally modelled natural patterns of GWTD are extracted from Fan et al. (2013). The model is forced by climate, terrain, sea level and GWTD observations (Fan et al., 2013). To

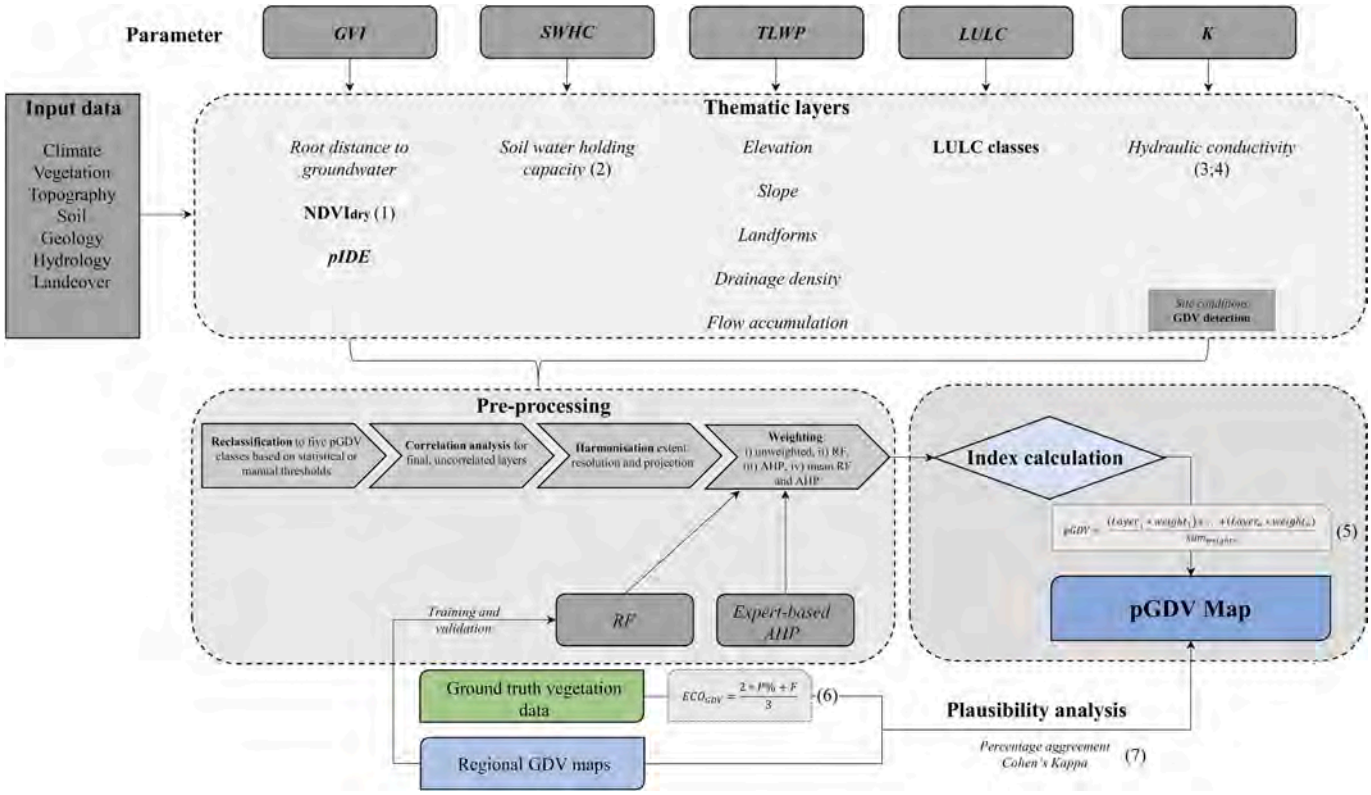

Fig. 1. Concept to map pGDV in the Mediterranean by integrating global datasets related to climate, vegetation, topography, soil, geology, hydrology and land cover. Eleven thematic layers addressing groundwater vegetation interaction (GVI), soil water holding capacity (SWHC), topographic landscape wetness potential (TLWP), land use and land cover (LULC) and hydraulic conductivity of rocks (K) are combined in the index. Layers either estimate favourable site conditions or allow for the detection of pGDV. The final pGDV map can be used to specify areas for high-resolution regional identification of GDV. The index can be adopted for other semi-arid environments. Numbers in brackets refer to the respective equations in the text. Abbreviations: ECO_{GDV} - Ecohydrological potential of GDV; P% - Phreatophyte coverage; F - Mean moisture value of non-phreatophyte species.

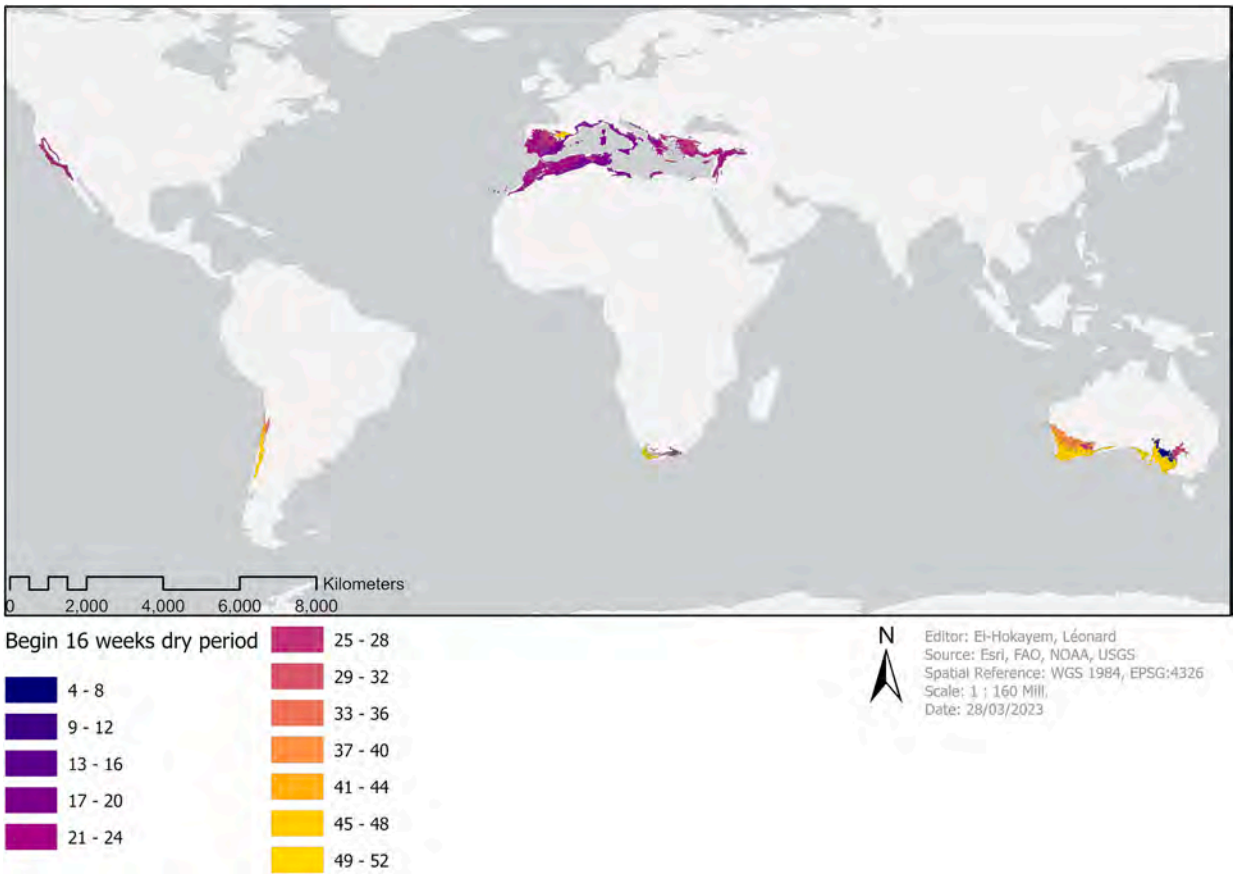

Fig. 2. Overview map of the Mediterranean biome and the beginning of the 16 driest weeks per year in 607 level 6 HydroBASINS (Lehner and Grill, 2013) calculated from daily CHIRPS precipitation data for the period 2003–2021.

account for the actual level of accessible water, capillary rise in different soil texture classes for the maximum depth available (200 cm) (Hengl, 2018) was added to the water table. Experimental results from Shen et al. (2013) are used to derive capillary fringe thickness in meters for each soil textural class. Defining thresholds for shallow GWTD as proposed e.g., by Doody et al. (2017) is not suitable on the biome scale due to the high alternation of rooting depth in different vegetation types (Canadell et al., 1996) and phreatophyte species (e.g., Lewis, 2011; Thomas, 2014). Fan et al. (2017) modelled the maximum depth of root-water uptake on a global scale. This model integrates soil water profiles (calculated from atmosphere, soil texture and topography), water demand of ecosystems and 2200 rooting depth observations. By subtracting modelled mean maximum depth of root water uptake (Fan et al., 2017) against the estimated level of groundwater capillary rise, we decided where groundwater uptake of plants is possible. Hence, values ≥ 0 imply that the deepest roots reach the modelled water table and may use groundwater.

2.2.1.2. NDVIdry. The application of multispectral RS-based indices allows the detection of trends and patterns of plant vitality which are crucial to identify pGDV (Eamus et al., 2006; Tweed et al., 2007; Pande et al., 2021). We utilised the mean NDVI (Rouse et al., 1974) (Eq. (1)) during the annual dry period between 2003 and 2021 ($NDVI_{dry}$) from MOD13Q1:

$$NDVI = \frac{\rho NIR - \rho Red}{\rho NIR + \rho Red} \quad (1)$$

where ρNIR represents the reflectance in the near-infrared and ρRed is the reflectance in the red visible band.

First, mean weekly precipitation was aggregated from daily CHIRPS data (Funk et al., 2015) for 607 HydroBASINS (level 6) (Lehner and Grill, 2013) over the period 2003–2021. The driest consecutive 16 weeks per basin were considered to represent annual dry periods. $NDVI_{dry}$ was calculated in GEE for the last 8 weeks of the respective dry period, when soil moisture stores are likely depleted and photosynthetic activity is more likely dependent on groundwater (Páscoa et al., 2020). According to the CGLS-LC100 land cover map (Buchhorn et al., 2020), cultivated and managed vegetation, urban areas, water bodies and moss and lichen were excluded from the analysis (Gou et al., 2015), as were pixels with mean NDVI values below 0.3 during the dry periods from 2003 to 2021 because they are unlikely to show natural pGDV (Páscoa et al., 2020). Finally, $NDVI_{dry}$ values were reclassified to five pGDV-classes in accordance with the final potentials, using unsupervised k-means clustering in GEE. Classes with high $NDVI_{dry}$ values are more likely to represent pGDV.

2.2.1.3. pIDE. Integration of climate data helps to highlight areas where climatic conditions indicate external water inflow. A simple ratio between mean annual ET derived from MOD16A3 (Running et al., 2017) and mean annual precipitation from CHIRPS was calculated for the period 2003–2021 in GEE to evaluate the pIDE of each pixel (Doody et al., 2017; Link et al., 2023). Pixels showing higher annual ET rates than actual precipitation are more likely to be groundwater-dependent (Doody et al., 2017). Thresholds for pIDE were adapted from Doody et al. (2017) to derive five pGDV classes.

2.2.2. Soil water holding capacity (SWHC)

Soils affect groundwater infiltration and thus groundwater recharge (Doody et al., 2017; Sun et al., 2018). Hence, SWHC depends on the type, texture and depth of the soil (Mollinedo et al., 2015). Physical soil

Table 1
Compilation of datasets used for the pGDV index. Input datasets are globally and openly available as well as ready-to-analyse and easy-to-use. Abbreviations: ET – Evapotranspiration; Prc – Precipitation; GWTD – groundwater table depth; Cf – Capillary fringe, Rd – Rooting depth; Perm – Intrinsic permeability; GWT – groundwater temperature; LULC – Land use land cover, Cl% – Clay content; Si% – Silt content; ST – Soil thickness; Dd – Drainage density; FA – Flow accumulation; LF – Landforms; Sl – Slope; El – Elevation.

Parameter	Factor	Application	Dataset	Spatial resolution	Unit	Data source
GVI	Climate (ET)	Calculation pIDE	MOD16A3	500 m	kg/m^2/ 8day	Running et al., 2017
GVI	Climate (Prc)	Calculation pIDE	CHIRPS 2.0	0.05 °	mm	Funk et al., 2015
GVI	Hydrogeology (GWTD)	Root distance to groundwater	Global Patterns of Groundwater Table Depth	30 s	m	Fan et al., 2013
GVI	Soil (Cf)	Root distance to groundwater	OpenLandMap Soil texture	250 m	m	Hengl, 2018
GVI	Vegetation (Rd)	Root distance to groundwater	Maximum depth root water uptake	30 s	m	Fan et al., 2017
GVI	Vegetation ($NDVI_{dry}$)	Vitality dry period	MOD13Q1	250 m	–	Didan, 2015
SWHC	Soil (Cl%)	Infiltration and storage of precipitation water	SoilGrids250 2.0	250 m	g/kg	Poggio et al., 2021
SWHC	Soil (Si%)	Infiltration and storage of precipitation water	SoilGrids250 2.0	250 m	g/kg	Poggio et al., 2021
SWHC	Soil (ST)	Infiltration and storage of precipitation water	Average Thickness of Soil, Regolith, and Sedimentary Deposit Layers	1 km	m	Pelletier et al., 2016
TLWP	Hydrology (Dd)	Low Dd implies high groundwater potential	Global Dd	Watersheds	km^{-1}	Lin et al., 2021
TLWP	Topography (FA)	Water movement on surface	MERIT Hydro	3 s	–	Yamazaki et al., 2019
TLWP	Geomorphology (LF)	Interaction between surface water and groundwater	Global SRTM Landforms	90 m	–	Theobald et al., 2015
TLWP	Topography (Sl)	Percolation of water into soil	SRTM	30 m	%	Farr et al., 2007
TLWP	Topography (El)	Groundwater availability	SRTM	30 m	m a.s.l.	Farr et al., 2007
LULC	Land cover	Classification and masking of LULC classes	CGLS LC100	100 m	–	Buchhorn et al., 2020
K	Geology (Perm)	Calculation K	GLHYMPS	10 km^2	m^2	Huscroft et al., 2018
K	Hydrogeology (GWT)	Calculation K	Global patterns of shallow groundwater temperatures	1 km	°C	Benz et al., 2017

properties such as clay (Cl%) and silt (Si%) content in the topsoil (0–30 cm) (Gomes Marques et al., 2019) were collected from SoilGrids250 2.0 (Poggio et al., 2021) and combined with global estimates of average soil thickness (ST) included from Pelletier et al. (2016) using Eq. (2).

$$SWHC = (Cl\% + Si\%)*ST \quad (2)$$

SoilGrids250 2.0 models global soil properties based on soil observations from 240,000 locations and environmental variables including vegetation, terrain, climate, geology or hydrology (Poggio et al., 2021). Pelletier et al. (2016) include topography, climate and geology to model soil thickness for different landform types. Thick soils with high shares of clay and silt allow the least infiltration and highest storage of water (Barbeta et al., 2015; Martínez-Santos and Renard, 2020) and thus are less likely to hold pGDV.

2.2.3. Topographical landscape wetness potential (TLWP)

Topographic-related parameters are commonly used predictors for the occurrence of GWPZ (Thanh et al., 2022) and pGDV, as they describe the accumulation and runoff of water (Martínez-Santos et al., 2021). Our approach to defining pixel-wise TLWP integrates elevation, slope and landforms with hydrological-related parameters on natural drainage density (Dd) and flow accumulation. Elevation and slope were acquired from the global SRTM digital elevation model (DEM) (Farr et al., 2007) in the GEE. Groundwater availability is often limited at higher elevations (Pande et al., 2021), whereas flat slopes generally indicate higher infiltration capacity (Gomes Marques et al., 2019) and thus low runoff and higher groundwater recharge (Magesh et al., 2012). SRTM-derived landforms based on hillslope position from Theobald et al. (2015) help to deduce groundwater movement and storage (Abijith et al., 2020) and hence the position of pGDV in the landscape. Valleys and flat slopes are related to water accumulation and support interaction between surface water and groundwater (Duran-Llacer et al., 2022). Peaks or ridges, on the other hand, support runoff and are therefore assigned low groundwater potential (Duran-Llacer et al., 2022; Pande et al., 2021). However, hydrological parameters complement topography-derived GWPZ (Thanh et al., 2022). For instance, natural drainage density, i.e., the length of streams within a specific area (Lin et al., 2021), is crucial to address groundwater availability. High Dd implicates less infiltration and hence lower groundwater potential (Arulbalaji et al., 2019). Global basin-wise Dd was extracted from Lin et al. (2021). The movement of water across the surface is represented by flow accumulation (Münch and Conrad, 2007), which is calculated in the MERIT hydro map from flow direction and describes the amount of the upstream catchment area (pixels) that drains into each pixel (Yamazaki et al., 2019). Hence, it allows for extracting pixels with high water accumulation such as stream channels but also wet areas that likely contain pGDV (Münch and Conrad, 2007). We adjusted thresholds for the five FA classes from Duran-Llacer et al. (2022) to target pGDV in the Mediterranean. Hence, pixels showing the highest flow accumulation (streams) are assigned the highest potential to include pGDV.

2.2.4. Land use land cover (LULC)

Hydrological dynamics such as infiltration or soil moisture, and hence groundwater availability, are affected by current LULC (Arulbalaji et al., 2019). LULC products allow locating classes such as forests, shrubland, urban areas or cropland and reclassifying them based on their likelihood to contain pGDV (Duran-Llacer et al., 2022). For our purpose we chose the CGLS-LC100 global land cover map from 2019 due to its high differentiation of 22 LULC classes, a resolution of 100 m and an overall accuracy of 80 % (Buchhorn et al., 2020). However, non-natural LULC classes (cultivated and managed vegetation, urban / built up) and water bodies were excluded from the final index to map natural pGDV only (Gou et al., 2015).

2.2.5. Hydraulic conductivity rocks (K)

The geological setting determines the existence of GWPZ in any terrain as infiltration depends primarily on the permeability of different rock types (Abijith et al., 2020). To directly account for permeability, we calculated K in m/s using Eq. (3) (Hubbert, 1956).

$$K = Ki^{*}g/v \tag{3}$$

where K is the hydraulic conductivity, K_i is the intrinsic permeability, g is the standard acceleration due to gravity (9.81 m/s^2) and v represents kinematic viscosity. Global intrinsic logarithmic permeability was extracted from Huscroft et al. (2018). Permeability was multiplied by 0.1 and the logarithm was solved to receive K_i in m^2 (Huscroft et al., 2018). Kinematic viscosity, calculated as a function of temperature and salinity, was derived following preceding studies (Dorsey, 1940; Weast, 1987). After obtaining values of kinematic viscosity in the common range of groundwater temperature (0 °C – 60 °C) and with a salinity of 0 ppm, a fourth-degree polynomial function ($R^2 = 0.99$) was applied to interpolate data and calculate global kinematic viscosity (v) in m^2/s from groundwater temperature (GWT) (Benz et al., 2017) (Eq. (4)).

$$\begin{aligned} v = {} & (4.3\,e\hat{}(-9)^{*}(GWT)\hat{}4 - 2.1e\hat{}(-6)^{*}GWT\hat{}3 \\ & + 4.1\,e\hat{}(-4)^{*}(GWT)\hat{}2 - 3.6\,e\hat{}(-2)^{*}GWT + 1.6\,)^{*}0.000001 \end{aligned} \tag{4}$$

In general, high hydraulic conductivity of the upper geological layer indicates deeper infiltration of water and reduced accessibility of groundwater for plants.

2.3. Weighting of thematic layers

Weighting assessment is crucial to prioritise the importance of several thematic layers for identifying pGDV (Doody et al., 2017; Duran-Llacer et al., 2022). In general, weight assessment accounts for the reliability of the different layers to identify pGDV as well as for the accuracy of the datasets used (Doody et al., 2017). Regional studies assume varying influence for several layers on pGDV's distribution and density and hence a strong need for weighting, especially in multicriteria analyses (Gomes Marques et al., 2019). However, the assignment of weights has a major impact on the uncertainty in multicriteria analyses and hence influences the final results (Fildes et al., 2023). We tested and combined the two most popular models used in GWPZ mapping (Thanh et al., 2022) to assign weights to each thematic layer and calculate different versions of the pGDV index to investigate how sensitive the final map accuracy is to different weightings. Expert-based AHP and predictive RF classifiers are presented in detail in the following sections.

2.3.1. Analytical Hierarchy Process (AHP)

Expert-based AHP (Saaty, 1986) is most commonly used in delineating GWPZ (Thanh et al., 2022), but was recently also used to map pGDEs regionally (Fildes et al., 2023; Rampheri et al., 2023). Following the procedure proposed by Rampheri et al. (2023), we decided on relative weights based on the mutual consensus, in our case the five authors from the fields of botany, hydrogeology, and remote sensing.

For each classified thematic layer, we defined relative weightings (single value per layer) according to the Saaty scale (1–9) in a pairwise comparison matrix (Arulbalaji et al., 2019; Pande et al., 2021) within an AHP (Goepel, 2018). Weightings were assigned in terms of environmental suitability for pGDV occurrence, pGDV detection and quality of the implemented datasets to address the influence on groundwater availability for plants (Pande et al., 2021). Weighting the layers is an iterative process considering known positions of GDV and weightings assigned in similar studies (e.g., Doody et al., 2017; Duran-Llacer et al., 2022; Gomes Marques et al., 2019) to calibrate the results. At last, the consistency of the pair comparisons is validated by a consistency ratio that should be ≤ 0.1 to continue the analysis (Saaty, 1990). AHP shows fast results but depends on expert opinion, thus the results are subjective (Thanh et al., 2022).

2.3.2. Random Forest (RF)

RF are predictive machine learning models that use an ensemble of uncorrelated decision trees to predict information, i.e., classes or values (Breiman, 2001). We trained three RF classifiers in three different Mediterranean regions, where information on potential or actual GDV locations was available. RF classifiers were used to predict modelled and known locations of GDV based on the eleven thematic layers. Potential GDV locations were extracted from studies in Australia (Doody et al., 2017), California (USA) (Klausmeyer et al., 2018) and the Iberian Peninsula (IP) (Páscoa et al., 2020). Because the studies differ in terms of GDV mapping methods (expert-based weighted pGDV index in Australia, habitat and species mapping in California, remote sensing pGDV based on NDVI time series in the IP), input data and final resolution, multiple RF were applied, also to analyse differences in layer importance in different regions.

We selected 500 random points across all GDV classes for each region, with two classes in California and the IP (low and high pGDV) and four classes in Australia (low, moderate, high, and very high pGDV). For each region, the plots were split into 80 % training and 20 % validation sets and a RF classifier was trained using the thematic layers as input. Non-natural LULC classes were masked before the implementation.

In a RF, the Gini impurity index was used to measure the importance of each feature (thematic layers) in the model. Gini impurity measures the probability of misclassifying a randomly chosen variable. Features with a larger decrease in Gini impurity are more important because they result in more homogeneous subsets (Breiman, 1984). Finally, the relative importance of each layer was extracted from the trained classifier (Murmu et al., 2019; Singh et al., 2013) and assigned as mean value over all regions (RF_mean). Additionally, the mean of weightings derived from AHP and RF_mean was calculated for each layer to combine expert-based and statistical approaches (AHP_RF).

2.4. Index calculation

To calculate the pGDV index, eleven thematic layers targeting GVI, SWHC, TLWP, LULC and K were overlaid in a novel multicriteria index. Firstly, pre-processing of the single layers include reclassification, correlation analysis, harmonisation and weight assessment. Therefore, input vector data such as Dd and intrinsic permeability were rasterized. Subsequently, all thematic raster layers were reclassified to five classes to estimate the potential of each pixel for the presence of pGDV (very high (5) to very low (1)) using statistical or manual thresholds. No data pixels are classified as 0. The distinction of five classes was not possible for RDGW, K and LF. Hydraulic conductivity (K) was reclassified based on existing thresholds (Freeze & Cherry, 1979) that define aquifer, aquitard and aquiclude. RDGW shows if the deepest roots reach the groundwater table or not. Intermediate classes were not distinguished.

Pearson correlation, derived from 'ArcGIS Multivariate Tool', was below 0.5 for all thematic layers, which indicates independency of the index variables. Consequently, all initial considered layers are included in the final index calculation (Duran-Llacer et al., 2022).

After reclassification and correlation analysis, input layers were harmonised in terms of extent, resolution (500 m) and projection (WGS 1984, EPSG:4326) using the *spatial_sync_raster* function (nearest neighbour interpolation) in the R-package 'spatial.tools' (Greenberg, 2021). All eleven layers and their respective class boundaries are summarised in Table 2. The derived classes represent potentials for each layer to either hold or identify pGDV.

Eq. (5) shows the final index that overlays all thematic layers and their respective weightings to identify pGDV. We calculated four different versions of the pGDV index with varying weights derived from 1) AHP; 2) RF_mean; 3) AHP_RF and 4) unweighted (see Section 2.2.6).

$$pGDV = \frac{\left((RDGW^{*}w_1) + \left(NDVI_{dry}{}^{*}w_2\right) + (pIDE^{*}w_3) + (SWHC^{*}w_4) + (El^{*}w_5) + (Sl^{*}w_6) + (LF^{*}w_7) + (Dd^{*}w_8) + (FA^{*}w_9) + (LULC^{*}w_{10}) + (K^{*}w_{11})\right)}{\sum_{i=1}^{11} w_i} \quad (5)$$

The resulting pGDV values were masked against the LULC layer, excluding cropland, urban areas, bare areas and water bodies, to map natural pGDV only. All remaining pixels were reclassified into five classes (very low to very high pGDV) using Jenks natural breaks (Gomes Marques et al., 2019) in each region (Mediterranean Basin, Chilean Matorral, California, South Africa, Australia) separately, to account for differences in vegetation (Pignatti, 2003), phreatophyte species (e.g., Gomes Marques et al., 2019; Lewis, 2011; Thomas, 2014) and environmental characteristics derived from the thematic layers between the regions. Areal shares of high and very high pGDV were finally calculated for level 8 HydroBASINS (Lehner and Grill, 2013) and reclassified to quartiles.

Table 2
Reclassification of the input thematic layers according to their potential of GDV occurrence based on statistical (quantiles, Jenks natural breaks, k-means) or manual classes.

Thematic layer	Method	Class boundaries	Rank
Root distance to groundwater	Manual	≥ 0	5
		< 0	1
$NDVI_{dry}$	k-means	*centroids*	
		0.78	5
		0.64	4
		0.52	3
		0.42	2
		0.34	1
Potential inflow dependency	Manual (Doody et al., 2017)	> 1.22	5
		≤ 1.22	4
		≤ 1.10	3
		≤ 0.99	2
		≤ 0.90	1
Soil water holding capacity	Quantiles	≤ 38.8	5
		≤ 58.1	4
		≤ 445.7	3
		≤ 1608.5	2
		≤ 4941.6	1
Elevation [m a.s.l.]	Natural breaks	≤ 278	5
		≤ 674	4
		≤ 1170	3
		≤ 1943	2
		≤ 4658	1
Slope [°]	Natural breaks	≤ 1.9	5
		≤ 6.9	4
		≤ 13.0	3
		≤ 20.8	2
		≤ 59.0	1
Landforms	Manual	valley	5
		lower slope (flat)	4
		upper slope (flat); lower slope	3
		peak/ridge; mountain/divide; cliff; upper slope	1
Drainage density [km^{-1}]	Natural breaks	≤ 0.3	5
		≤ 0.5	4
		≤ 0.6	3
		≤ 0.8	2
		≤ 1.2	1
Flow accumulation [n cells]	Manual (Duran-Llacer et al., 2022)	> 5000	5
		100–5000	4
		20–100	3
		5–20	2
		0–5	1
Land use land cover	Manual	herbaceous wetland	5
		closed and open forest, evergreen broad leaf	4
		shrubs, other forests types	3
		herbaceous vegetation	2
		bare / sparse vegetation	1
		cultivated and managed vegetation, urban / built up, water bodies	mask
Hydraulic conductivity [m/s]	Manual (Freeze & Cherry, 1979)	≤ 1e-8	5
		≤ 1e-6	3
		> 1e-6	1

2.5. Plausibility analysis

The plausibility analysis should allow the selection of the weighting model from the four different approaches, which then has been used for the final pGDV map for the Mediterranean biome. Therefore, we compared the results to GDV locations in Campania (El-Hokayem et al., 2023 and this study) and California (Klausmeyer et al., 2018) as well as to a pGDV layer for Australia (Doody et al., 2017). In California, GDV was mapped based on vegetation alliances, vegetation types, and habitat types and assessment of whether the dominant species is a phreatophyte (Klausmeyer et al., 2018). Doody et al. (2017) mapped pGDV based on water use of vegetation, shallow groundwater, low SWHC and GDV species using a weighted index. Resulting pGDV polygons were rasterized and harmonised to match our final index map.

Ground truth vegetation data was obtained from botanical field campaigns in Campania (Italy). In 2021, 116 vegetation plots (10 m × 10 m) were collected in low permeable terrains (El-Hokayem et al., 2023). In 2022, 120 plots (10 m × 10 m) were collected in low, medium and high permeable regions. For each plant species we assigned adapted Ellenberg (1974) moisture values (Pignatti et al., 2005), which are helpful to characterise ecological site conditions and hence groundwater dependency (Killroy et al., 2008). Each species was further classified as phreatophyte or not based on studies of phreatophyte species (e.g., Gomes Marques et al., 2019; Lewis, 2011; Thomas, 2014).

All vegetation plots were classified to represent GDV likelihoods using a simple ecohydrological rule set introduced in El-Hokayem et al. (2023) considering plot-wise phreatophyte coverage (P%) and mean moisture value of non-phreatophyte species (F). We adjusted the rule set to derive five final classes. Consequently, each plot was classified into five classes for P%: 1) non-GDV (P% < 1); 2) unlikely GDV (P% = 1–25); 3) as likely as unlikely GDV (P% = 25–50); 4) likely GDV (P% = 50–75); 5) GDV (P% > 75) and F: 1) non-GDV (F < 3 (arid)); 2) unlikely GDV (F = 3); 3) as likely as unlikely GDV (F = 4); 4) likely GDV (F = 5) and 5) GDV (F > 5 (well supplied with water)). Finally, the ecohydrological potential of GDV (ECO_{GDV}) was calculated from P% and F-derived classes (1–5) as follows:

$$ECO_{GDV} = \frac{2^{*}P\% + F}{3} \quad (6)$$

Locations that were used in the weight assessment with RF (Australia and California) were excluded prior to the plausibility analysis. We also first merged the five derived pGDV classes into two classes (very low to low and moderate to very high) to obtain a nominal scale. The same aggregation was applied for the reference data in Campania and Australia. Then, we calculated percentage agreement for the two classes compared to GDV locations in Campania (pGDV extracted for 236 vegetation plots) and pGDV in Australia (pixel-wise comparison of 527,244 pixels). Therefore, we divided the total number of correct pixels per class by the total number of pixels in that class as derived from the reference data (Congalton, 1991). As only polygons with mapped GDV exist for California, we calculated the proportion of moderate to very

high pGDV pixels in these polygons, which relates to 3203 pixels of our pGDV map.

Based on the percentage agreement, we finally calculated Cohen's Kappa (κ) to interpret interclass correlation. The κ measures the agreement between reference data and classification, while also accounting for chance agreement between classes and was calculated using Eq. (7) (Cohen, 1960).

$$\kappa = \frac{p_o - p_c}{1 - p_c} \tag{7}$$

where p_o is the observed agreement between raters and p_c is an estimation of the 'per chance' agreement. Despite, documented flaws in the use of κ to measure accuracy of classified images in RS (e.g., Foody, 2020; Pontius and Millones, 2011) we used κ, as we analysed the agreement beyond change (Foody et al., 2020) of nominally scaled pGDV maps.

3. Results

3.1. Thematic layers

Spatial patterns for each reclassified thematic layer in the Mediterranean biome are presented in Figs. 3-5.

Fig. 3 highlights those layers contributing to groundwater vegetation interaction (GVI). Patterns of shallow GWTD (≤10 m) explain 89 % of the pGDV, classified from RDGW, while deep roots (≥10 m) are found in 31 % of the high pGDV. High pGDV is extracted in all regions along river courses and around waterbodies in the inland. Moreover, wetlands and lagoons of river deltas, such as the 'Parc naturel régional de Camargue' in Southern France are classified as high pGDV. Large patterns where the GWTD exceeds rooting depth are located in Southern Maghreb, inland Australia and Northern Chile, which is in line with patterns observed for $NDVI_{dry}$. Based on $NDVI_{dry}$, 45 % of the natural vegetation pixels indicate low pGDV and 22 % show at least high pGDV. Pixels, with high pIDE are more commonly found in coastal areas. Thus, 90 % of the pixels are not inflow dependent, as ET is lower than precipitation. Contiguous areas with high pIDE can be found on the Greek coast and islands in the Aegean Sea and the Californian coast, also in accordance with high $NDVI_{dry}$ and low RDGW. A belt of high pIDE is present in the Southern Atacama Desert in Chile which is not pronounced for $NDVI_{dry}$ or RDGW.

Fig. 4 highlights pGDV locations suggested by geology, soils, and land cover. Large patches of favourable soil conditions for groundwater recharge and hence pGDV can be found on thin and sandy soils in the North-Western part of the IP, West-Australia, South Africa and the Southern part of the Maghreb, i.e., on Regosols, Leptosols or Arenosols (Poggio et al., 2021). However, regions with water-holding soils are concentrated e.g., in Eastern Australia or in the high steppe plateaus between Morocco and Algeria and make up around 30 % of the whole Mediterranean.

LULC classes indicating cultivated and managed vegetation, urban areas or water bodies (29 % of the Mediterranean area) were excluded from our analysis. Bare lands with low pGDV can be found in Southern Maghreb and the Atacama Desert in Chile. For 41 % of the area, moderate potentials were assumed, as no further discrimination of pGDV was possible from the given LULC classes. Larger areas of evergreen trees that may depend on groundwater usage are located in Western Australia and Southern Chile but represent only 1 % of the total area. Those areas in Western Australia have also high potentials for GVI.

Patterns of low permeability and expected shallow groundwater circulation derive from hydraulic conductivity. Low to high potentials for pGDV are distributed throughout the whole biome, often in close proximity. However, 27 % of the lithological units are likely to hold pGDV, such as in central Spain or South Africa, where sedimentary rocks predominate. For 53 % of the Mediterranean, the suitability for pGDV is low due to geology, e.g., in carbonate sedimentary rocks in Western Australia and Italy, or volcanic rocks in Chile (Hartmann and Moosdorf, 2012).

Layers determining TLWP are presented in Fig. 5. Higher altitudes and expected lower pGDV can be found primarily in Atlas, Andes, Apennines or Taurus mountains. Here, steep slopes >20.8° also indicate surficial runoff and less recharge. Whereas, coastal areas, Australia, Southern Chile and the Western part of the IP are characterised by altitudes below 674 m a.s.l. and flat slopes, favouring the presence of pGDV. Preferable geomorphological conditions for pGDV are refined in the IP and Maghreb. Watersheds along the coastline of the Mediterranean Basin, South Africa or Australia show low Dd, while inland areas in

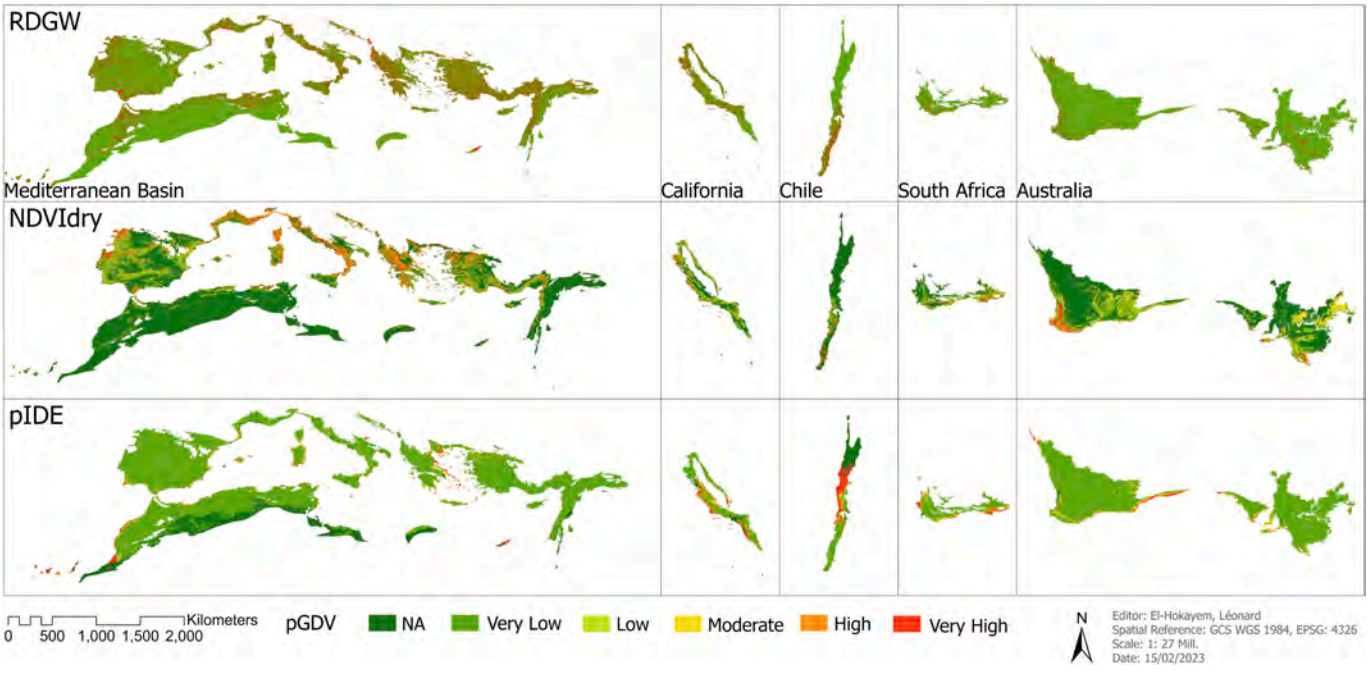

Fig. 3. Thematic layers that indicate groundwater vegetation interaction (GVI) in the five Mediterranean sub-regions. RDGW = Root distance to groundwater; $NDVI_{dry}$ = Normalized Difference Vegetation index in the dry period; pIDE = potential inflow dependency.

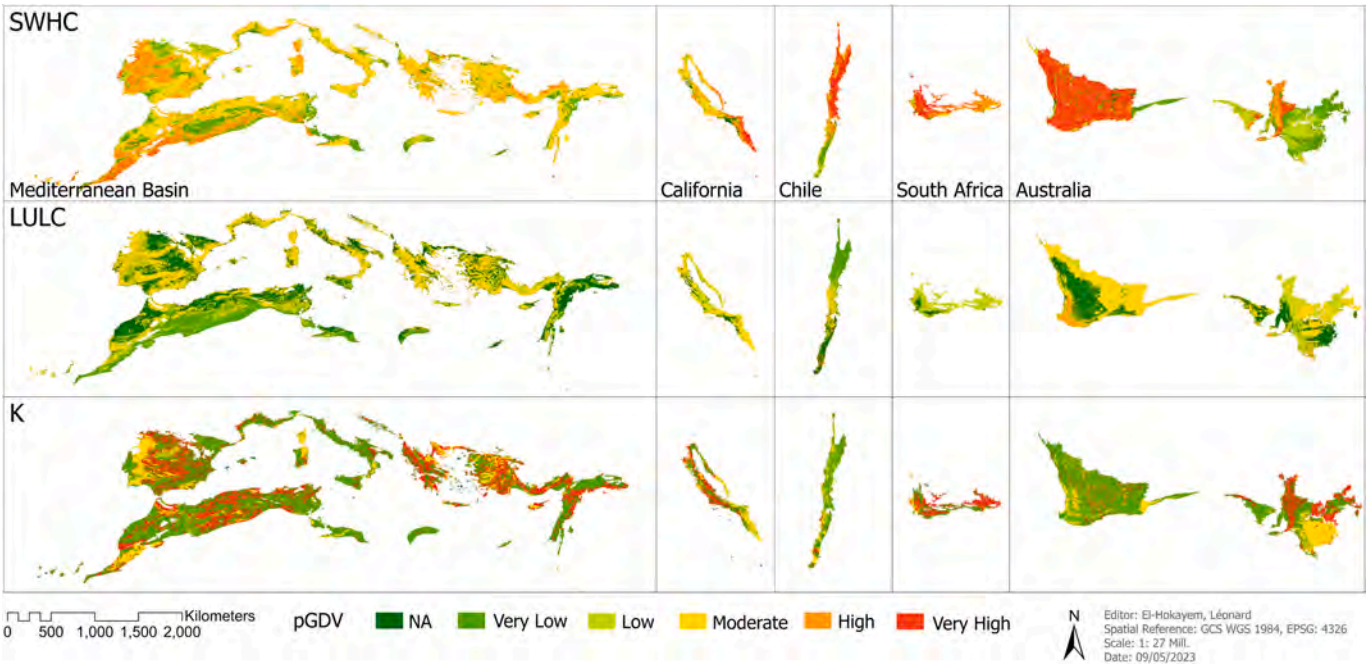

Fig. 4. Thematic layers that indicate soil water holding capacity (SWHC), land use land cover (LULC) and hydraulic conductivity of rocks (K) in the five Mediterranean sub-regions.

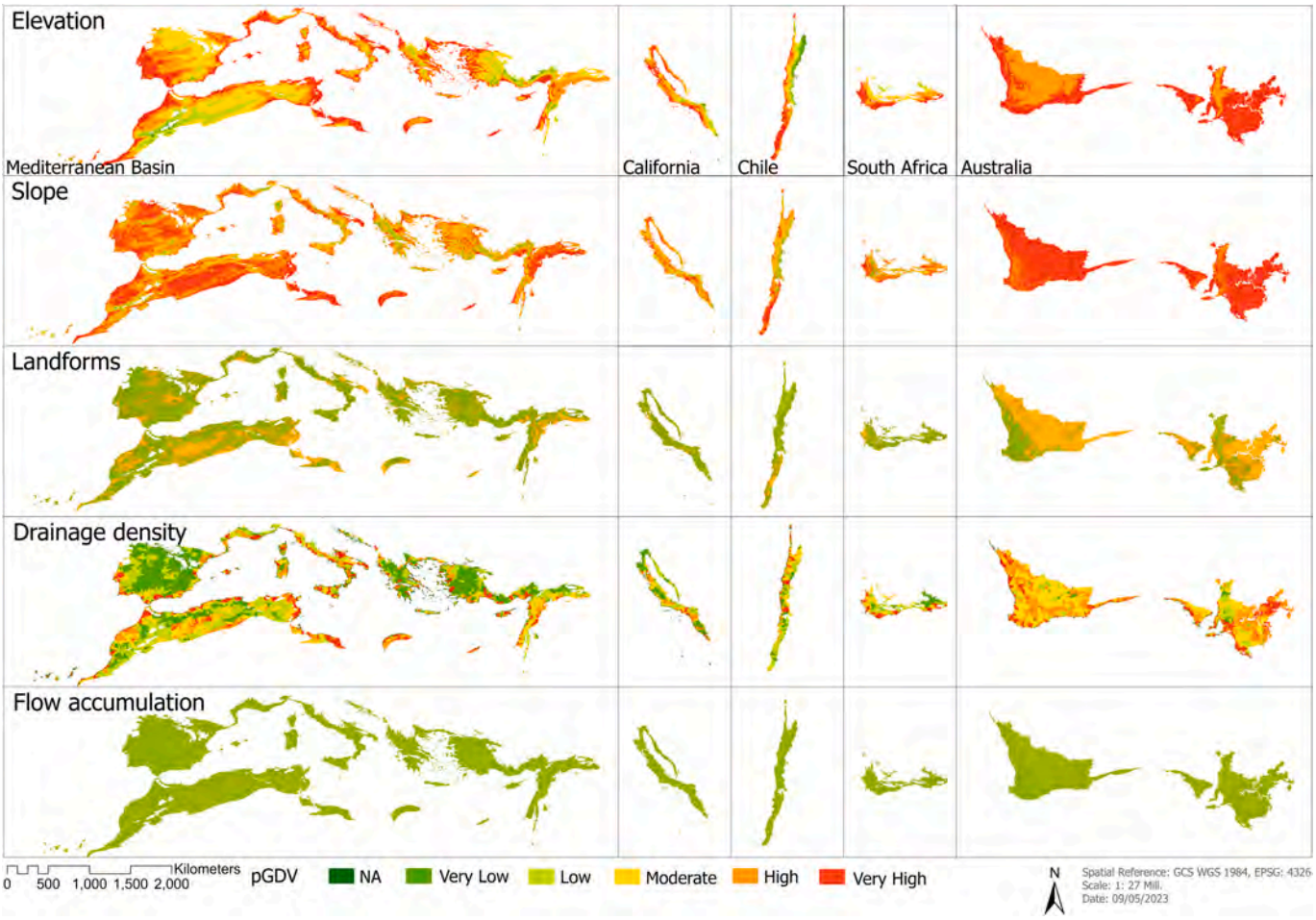

Fig. 5. Thematic layers that indicate topographic landscape wetness potential (TLWP) in the five Mediterranean sub-regions.

Table 3
Pairwise comparison matrix used in the AHP to calculate respective weightings between eleven thematic layers based on expert opinion. Values range between 0.25 (row layer strongly less important than column layer) to 4 (row layer strongly more important than column layer). The consistency ratio was 0.048, hence the comparisons are consistent and derived weightings are reliable.

Thematic layer	pIDE	RDGW	$NDVI_{dry}$	SWHC	FA	LF	Sl	El	Dd	LULC	K
pIDE	1	3	0.33	1	1	1	2	3	3	2	3
RDGW	0.33	1	0.25	1	0.5	1	3	3	3	0.5	2
$NDVI_{dry}$	3	4	1	2	1	3	3	4	4	2	3
SWHC	1	1	0.5	1	0.5	1	1	2	3	2	2
FA	1	2	1	2	1	1	3	4	3	2	3
LF	1	1	0.33	1	1	1	3	3	2	2	3
Sl	0.5	0.33	0.33	1	0.33	0.33	1	4	1	1	2
El	0.33	0.33	0.25	0.5	0.25	0.33	0.25	1	0.5	0.33	0.5
Dd	0.33	0.33	0.25	0.33	0.33	0.5	1	2	1	2	1
LULC	0.5	2	0.5	0.5	0.5	0.5	1	3	0.5	1	1
K	0.33	0.5	0.33	0.5	0.33	0.33	0.5	2	1	1	1

Table 4
Weightings of all thematic layers derived from variable importance of RF classifiers trained by available pGDV maps from Australia, the Iberian Peninsula and California (see Section 2.3). pGDV locations originate from maps in Doody et al. (2017); Páscoa et al. (2020) and Klausmeyer et al. (2018).

Region	pIDE	RDGW	$NDVI_{dry}$	SWHC	FA	LF	Sl	El	Dd	LULC	K	Training accuracy	Validation accuracy
Australia	6.0	3.5	10.3	12.1	16.0	13.0	5.5	3.7	13.9	6.6	9.5	0.73	0.51
Iberian Peninsula	4.1	6.1	14.4	10.1	12.8	10.7	9.6	9.3	11.4	2.7	8.5	0.74	0.59
California	10.0	4.7	12.1	9.5	12.1	8.5	7.2	8.7	13.0	5.2	9.0	0.94	0.82

Table 5
Final weights for all thematic layers derived from AHP, RF_mean and AHP_RF used for the different pGDV maps. In the unweighted version, all layers have been given a weight of 1.

Weighting method	pIDE	RDGW	NDVIdry	SWHC	FA	LF	Sl	El	Dd	LULC	K
AHP	12.1	8.5	19.9	9.2	14.1	10.7	6.1	3.0	5.1	6.7	4.5
RF_mean	6.7	4.8	12.3	10.1	12.8	10.8	7.4	7.3	12.8	4.8	9.0
AHP_RF	9.4	6.7	16.1	9.7	13.5	10.8	6.8	5.2	9.0	5.8	6.8

Turkey, Greece and the IP have high Dd. Areas of concentrated flow (high FA) such as streams are distributed in the whole biome and make up 16 % of the area. In general, patterns of high FA resemble landforms with high pGDV such as valleys. Nevertheless, FA still refines pixels towards which surface water flows and is more likely to accumulate. Low FA and thus decreased water availability were classified for 67 % of the pixels.

3.2. Weightings from AHP and RF

Detailed results from both weighting approaches (AHP and RF) are presented in Tables 3 and 4. Additionally, Table 5 summarises the weightings applied for the biome-wise map.

Highest mean weightings from AHP and RF_mean were calculated for $NDVI_{dry}$ (16.1), FA (13.9), LF (10.7) and pIDE (9.4). However, differences exist between both weight assessments (AHP and RF_mean) as well as across the different Mediterranean regions. The highest variations between the methods are found for Dd and elevation and K where weightings from RF_mean are twice as high as from AHP. Importance found for FA and LF highly resemble each other. Across the regions, RF_mean weightings widely differ for pIDE, slope and elevation.

3.3. Plausibility analysis

The plausibility of the results varies depending on assessed layer weightings compared to GDV locations or potentials in Campania (CAM), California (CAL) and Australia (AUS) (Table 6). Compared to AUS, results from the unweighted index show the highest consistency of pixels indicating at least moderate pGDV. However, the comparison suggests an overestimation of pGDV, as 80 % of low pGDV pixels in AUS are assigned to higher potentials, resulting in poor agreement according to κ. Depending on the applied weightings, 86 % to 99 % of likely GDV or GDV in CAM were located in areas with at least moderate suitability for the occurrence of pGDV. Based on κ, a moderate agreement (0.41) is presented for the unweighted index. Also, for CAL, the highest plausibility was found using the unweighted index, as only 13 % of the GDV area is located in regions indicating very low to low pGDV, and good agreement was derived.

Table 6
Percentage agreement of pGDV maps based on different layer weightings from AHP, RF_mean, mean of AHP and RF_mean (AHP_RF) and unweighted with GDV locations (Campania: CAM, California: CAL) or pGDV (Australia: AUS). Numbers for AUS and CAM present the percentage of pixels in which the merged classes match. The proportion of moderate to very high pGDV classes inside mapped GDV polygons is shown for CAL. Cohen's kappa (κ) expresses the level of agreement.

Dataset	Type	Classes	AHP [%]	AHP_RF [%]	RF_mean [%]	unweighted [%]
AUS	pGDV (pixel)	Very low – low	44.1	40.3	32.2	19.8
		Moderate – very high	53.6	59.1	66.6	79.2
		κ	−0.06	−0.09	−0.16	−0.27
CAM	pGDV field surveys (plot)	Very low – low	8.6	18.5	33.3	32.1
		Moderate – very high	99.0	99.0	86.1	91.1
		κ	0.34	0.40	0.37	0.41
CAL	GDV locations (polygon)	Moderate – very high	73.6	76.2	76.9	86.7
		κ	0.53	0.58	0.59	0.76

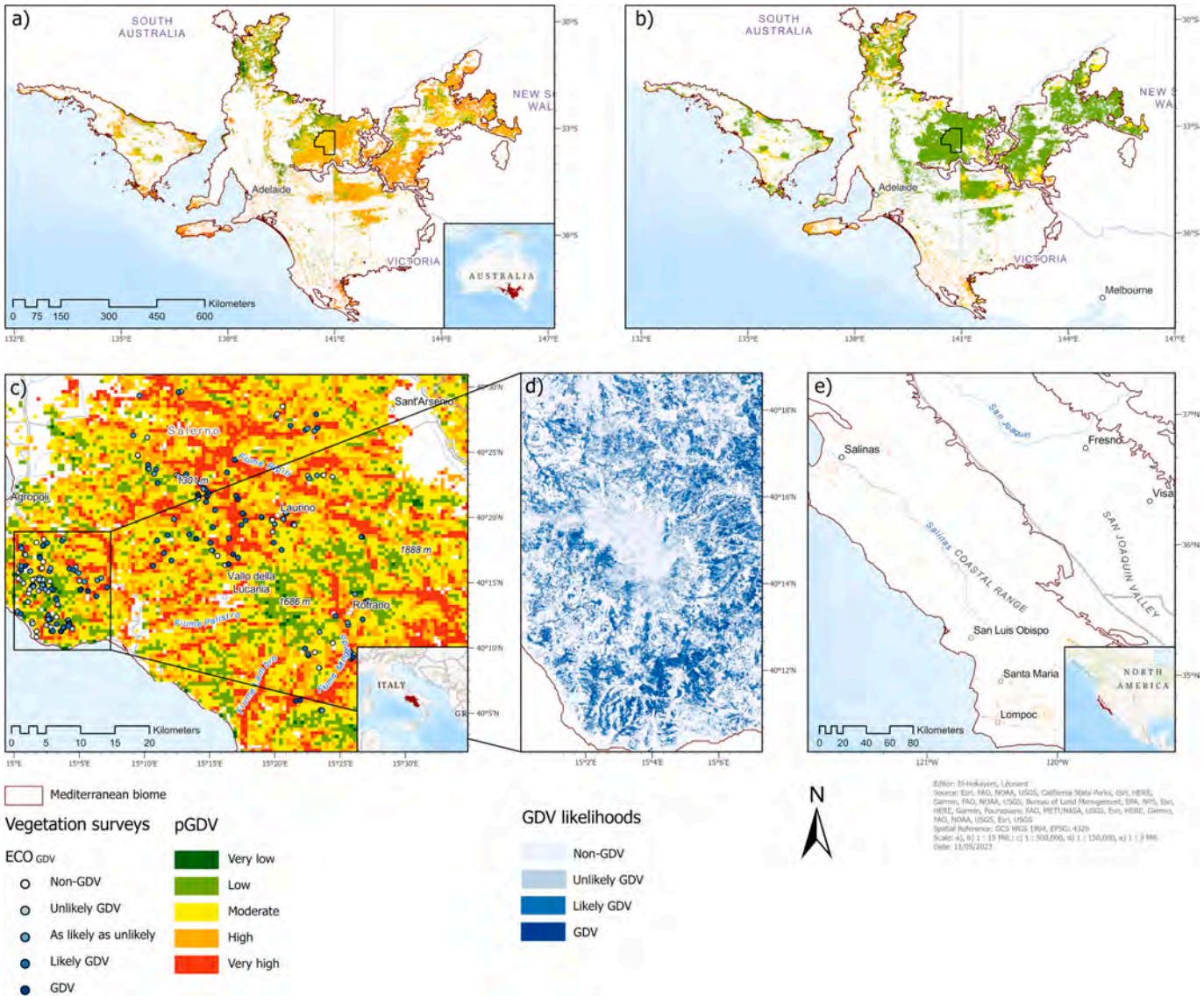

Fig. 6. Plausibility analysis of a) pGDV from the unweighted index calculation against b) the pGDV layer of Australia (Doody et al., 2017); c) pGDV field surveys in the 'Cilento, Vallo di Diano and Alburni National Park' and d) a high-resolution GDV likelihood map for the 'Mount della Stella' area in Campania (Italy) (El-Hokayem et al., 2023); e) GDV locations in California (USA) (Klausmeyer et al., 2018). In a) and b) the 'Danggali Conservation Park' (Australia) is highlighted (relevant for discussion).

Compared to AUS, results from the unweighted index show the highest consistency of pixels indicating at least moderate pGDV. However, the comparison suggests an overestimation of pGDV, as 80 % of low pGDV pixels in AUS are assigned to higher potentials, resulting in poor agreement according to κ. Depending on the applied weightings, 86 % to 99 % of likely GDV or GDV in CAM were located in areas with at least moderate suitability for the occurrence of pGDV. Based on κ, a moderate agreement (0.41) is presented for the unweighted index. Also, for CAL, the highest plausibility was found using the unweighted index, as only 13 % of the GDV area is located in regions indicating very low to low pGDV, and good agreement was derived.

Fig. 6 shows a spatial comparison between the unweighted pGDV index and the AUS, CAM and CAL maps. From a conservative point of view, it showed the highest agreement (CAL and CAM) with known GDV locations and high pGDV (AUS).

3.4. Final pGDV map

The final pGDV map and frequency distributions of different pGDV levels and area shares of high pGDV per basin are shown in Fig. 7. Regions with high pGDV are distributed throughout the Mediterranean biome. Occurrence increases in coastal areas and along riverine landscapes. 31 % of the natural vegetation in the Mediterranean shows a high potential to be GDV. Moderate potentials were calculated for 37 % and 32 % have low or very low potentials. However, 11 % of 5331 level 8 HydroBASINS (Lehner and Grill, 2013) in the biome have an area share of pGDV above 50 %.

4. Discussion

4.1. Global geodata and thematic layers

Global datasets were selected for this study based on the findings on appropriate thematic layers for pGDV identification (see Chapter 2). The use of global datasets can overcome data coverage issues, and recently published datasets (e.g., Fan et al., 2013; Fan et al., 2017; Yamazaki et al., 2019) can improve the quality of global analyses. However, there remains a trade-off between the level of detail required and data

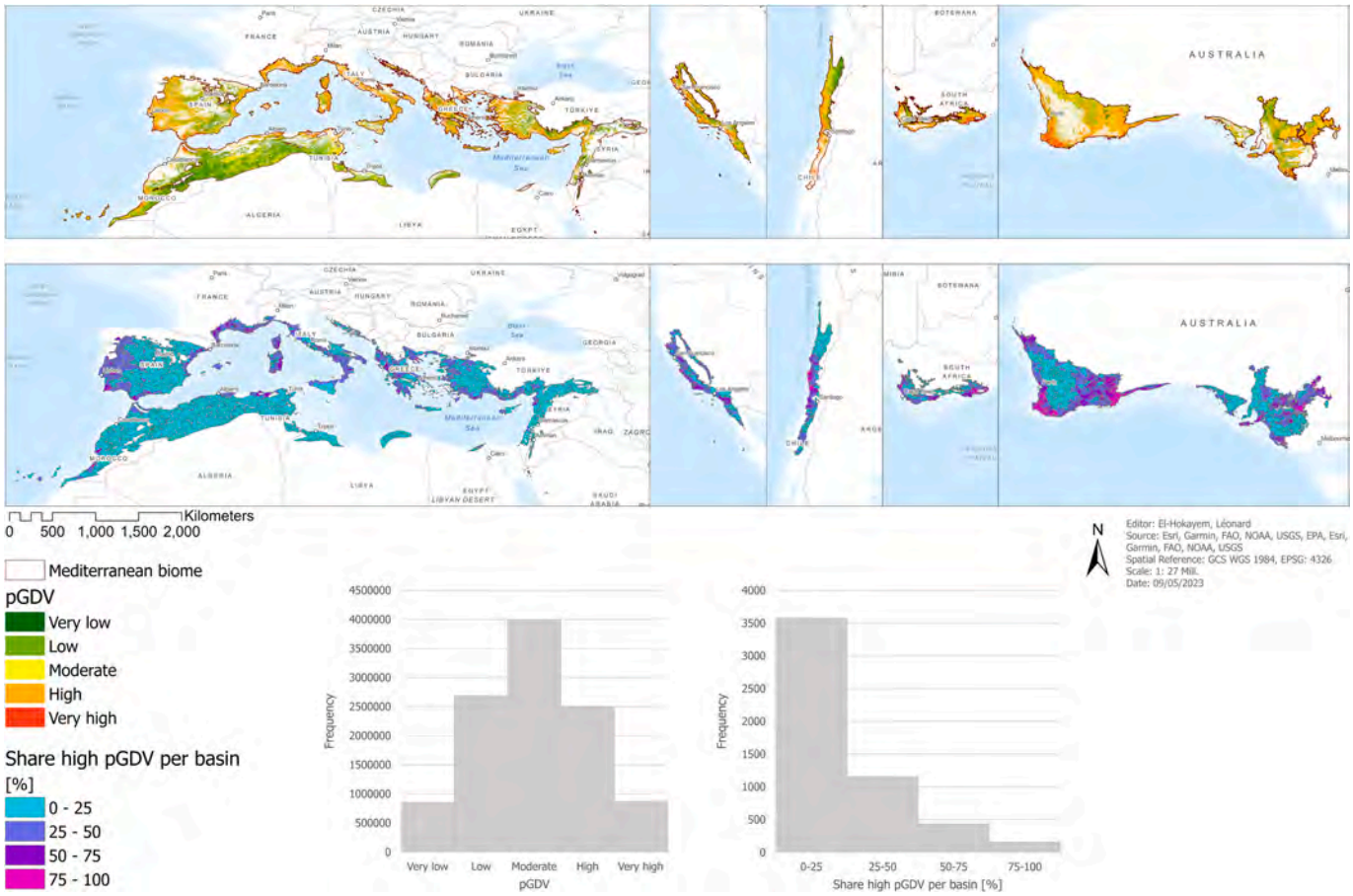

Fig. 7. Final Mediterranean pGDV map at 500 m resolution based on the unweighted index.

availability. For instance, the resolution of global faults extracted by Styron & Pagani (2020) is too coarse to match the expected spatial variability of GDV. As a consequence, regions with high groundwater potential due to fractured aquifer potential (Münch and Conrad, 2007; Duran-Llacer et al., 2022) could not be included in the index calculation.

Other global datasets may have had weaknesses, which the automated weighting approaches with RF or plausibility analysis ultimately revealed. The availability of datasets on GWTD (Fan et al., 2013), rooting depth (Fan et al., 2017) and capillary rise (Hengl, 2018) has allowed us to more directly account for root access to groundwater (RDGW) over larger areas, where the utilisation of one threshold for shallow GWTD was insufficient (see Section 2.2.1). The RF-based approaches clearly underestimated this relevant parameter, which in turn raises the question of introducing weightings at the sub-biome level, as used for ecozones in Australia (Doody et al., 2017). Nevertheless, the application of the approach leads to plausible results at the global level, as shown by the plausibility analysis and confirmed by the study of Link et al. (2023) on global pGDE. Other aspects, such as unevenly distributed training data (e.g., Fan et al., 2017; Poggio et al., 2021), errors in LC100 LULC classes that are not associated with natural GDV but are likely to be detected by the pGDV index (e.g., irrigated cropland, waterbodies), upscaling of detailed LULC information, or downscaling of hydroclimatic data may be potential sources of uncertainty that global datasets introduce into the global index.

In terms of computational and storage requirements, continuous medium-scale NDVI time series were compiled from MODIS data, although high-resolution Landsat or Sentinel-2 time series used by Box et al. (2023) or Gou et al. (2015) on local scales, could have increased the spatial accuracy of the results. The plausibility analysis shows clear signs of overestimation of pGDV, which could be explained by the identification of e.g. drought-tolerant species that do not use groundwater but still maintain a constant vitality during a dry period, or areas with a persistent water supply from soil water (Gomes Marques et al., 2019).

Although, several global datasets (e.g., CHIRPS 2.0, Global Patterns of Groundwater Table Depth, Maximum depth root water uptake, SoilGrids250 2.0) rely on similar input parameters and data for modelling, no intercorrelation was found between the reclassified thematic layers, in contrast to studies by Gomes Marques et al. (2019) or Duran-Llacer et al. (2023). In addition, the limited coastal coverage of some data (e.g., Benz et al., 2017; Lin et al., 2021) resulted in missing values and underrepresentation of pGDV in these areas with high probability of GDV occurrence (Doody et al., 2017).

4.2. *RF-based weights from regional data sets*

As mentioned in Section 2.3.2, it was not possible to derive a global RF model due to the differing training data of the included regional studies. Nevertheless, and despite the variations considered by the ecozone-wise weighting proposed by Doody et al. (2017), similar weightings would have been expected at the biome scale. However, the characteristics of individual thematic layers vary from region to region. For instance, small variations in elevation or slope in Australia (see Fig. 5) resulted in a lower weight, while large variations in pIDE in California (see Fig. 4) have led to a higher weight (Table 4). These variations are due to the fact that RF fits the parameter expressions of the training data. On the other hand, the random selection of training points may not represent all variations in the thematic layers, resulting in known overfitting issues of RF (Belgiu and Drăguţ, 2016).

However, in particular K, SWHC, Dd, and SI show similar weightings

across the regions (Table 4) and hence were evaluated to influence the occurrence of pGDV formed by azonal phreatophyte vegetation in a similar way. The averaging (RF_mean) finally tested for the global pGDV index can be seen as a compromise, as it can compensate for over- and underestimations of weights at the regional scale.

Classification accuracies derived from RF are low for pGDV estimated for Australia (Doody et al., 2017) or the IP (Páscoa et al., 2020) compared to those for actual GDV locations in California (Klausmeyer et al., 2018), which reach a remarkably high level (Table 4). At first glance, this suggests that, at least for the RF-based approach presented, it is preferable to derive weights from actual GDV locations, which are primarily produced by taking field data into account, rather than using other pGDV datasets, which are inherently subject to uncertainty. However, it must be added that the resolution of the datasets used, the availability of the datasets and the different target (pGDE instead of pGDV), especially for the Australian dataset, as well as the possibly oversimplified, purely RS-based approach for the IP (Páscoa et al., 2020) were most likely also reasons for the low accuracy of these RF models.

4.3. Global weights (AHP and RF_mean)

In general, expert-based weights show notable differences depending on whether GDV, GDE or GWPZ is the subject of the analysis. As the proposed index focuses on vegetation, plant vitality in the dry period ($NDVI_{dry}$) was given the highest weight in the AHP. The results are similar to the AHP of Fildes et al. (2023), who also point to improved RS technology as a reason for prioritising, for example, vegetation indices over ecosystem-characterising site conditions. Nevertheless, and especially when appropriate thematic layers are available, geology, precipitation and landforms are given the highest importance in pGDE (e.g. Duran-Llacer et al., 2022) or GWPZ mapping (e.g. Pande et al., 2021).

RF-based results suggest that AHP overestimates the influence of $NDVI_{dry}$ and pIDE (Table 5). Similarly, AHP assess drainage density to be less important for mapping pGDV globally, e.g. due to its coarse aggregation at the catchment scale. Nevertheless, it was found to be the second most important weight in RF_mean. Also, in comparison with available regional studies, RF_mean and AHP showed different weightings. For AUS, GWTD is given the highest weight and the occurrence of known groundwater dependent species is the least important. (Doody et al., 2017). Similarly, the RDGW, i.e. the parameter adapted for global application, ranks fifth in the AHP, certainly slightly downgraded by the experts' knowledge of its very strong generalisation. Conversely, based on the RF_mean used for weighting, RDGW is among the least important variables for predicting pGDV in this study. This was also observed by Gomes Marques et al. (2019) and can most likely be explained by poor data quality and the limitations of the globally modelled natural groundwater levels and rooting depths (see Section 4.1), which can hardly represent all local variations and anthropogenic impacts.

As suggested by Gomes Marques et al. (2019), regression analysis can help overcome the problems of expert-based weighting to assign appropriate weights to thematic layers when modelling pGDV. However, due to the spatial variance of thematic layers, upscaling the approach to regional or even biome scale may not provide adequate results, as it requires appropriate adjustment to local environmental conditions.

4.4. Final pGDV map and its application

The final map at 500 m resolution is crucial to delineate regions with high pGDV in the Mediterranean. However, smaller pGDV patterns are not detected. The final map for the Mediterranean provides information on pGDV for a given time section (2003−2021). Vegetation using groundwater outside of this period or vegetation affected by drought or fire may not have been identified as pGDV. The map confirms that pixels indicating natural vegetation in low permeable valleys or at low slope areas, where water accumulates and GWTD is shallow, which also show high vitality during the annual dry period and high pIDE while SWHC is low, are hence most likely to include pGDV.

The unweighted index performs well in delineating pGDV at expected GDV locations. For example, similar distribution patterns of pGDV derived from the index were observed in comparison to a local study in Southern Italy (see Fig. 7) based on high-resolution Sentinel-2 timeseries analysis and local DEM data (El-Hokayem et al., 2023). However, after iterative weighting and adjustment of input data, pGDV occurrence is still overestimated, especially compared to the AUS pGDV layer, which may be due to differences in weights, thresholds and the aggregation of moderate to very high pGDV classes for the plausibility analysis. The differences observed in Australia are striking, where there is considerable variation between areas of low pGDV (Doody et al., 2017) compared to moderate or high pGDV estimates derived from the index. To compare both maps against the backdrop of limitations of the Australian map (e.g., limited coverage, incomplete datasets, large polygons) (Doody et al., 2017), we assessed the water use of the vegetation present in the 'Danggali Conservation Park' (see Fig. 6) and compiled a species list from 'NatureMaps' (Government of South Australia, 2023). Out of the ten most prevalent species, eight are linked to GDV (e.g., *Dodonaea viscosa*, *Senna artemisioides*, *Olearia pimeleoides*, *Atriplex stipitate*) (Department of Environment and Science, Queensland, 2013), indicating that the prevalence of pGDV may be higher than estimated by the broad-scale assessment in the Australian pGDE Atlas (Doody et al., 2017).

The accuracy of the pGDV index is limited by parameters that favour the occurrence of GDV instead of parameters that control the detection of GDV. In many regions the environmental site conditions may be suitable for pGDV occurrence although GDV is not present, which could explain the observed overestimation, as also reported by e.g., Box et al. (2022), El-Hokayem et al. (2023), and Fildes et al. (2023).

As GDV is globally distributed and threatened, particularly in the Mediterranean biome, the novel global pGDV map of the Mediterranean biome can support their detection and management. For instance, the Mediterranean pGDV map can be used by regional authorities or researchers to select regions of interest where the proportion of pGDV is high and a detailed analysis of GDV is required, i.e. the combination of ground-based identification and high-resolution RS as shown e.g. by Klausmeyer et al. (2018) or El-Hokayem et al. (2023) is required. Overlaying maps with predicted groundwater declines, e.g. du to pumping or climate change, can, for instance, help to identify areas in need of biodiversity protection.

5. Conclusion

This study proposes a novel easy-to-use multicriteria index to identify pGDV in the Mediterranean biome. The index integrates global geodata from different sources, complementing regional models on GWPZ with vegetation-related parameters to map pGDV at the biome scale. Eleven thematic layers are combined, targeting groundwater vegetation interaction, soil water holding capacity, topographic landscape wetness potential, land use land cover and hydraulic conductivity of rocks. Overlaying environmental conditions together with vegetation dynamics and characteristics allows the determination of pGDV.

The discussion underpinned that expert-based weighting from AHP can be subjective and hence prone to bias. On the other hand, RF can only be applied if there is sufficient training data to provide reasonable weighting. Thus, the results of the plausibility analysis imply that the overall weighting or general classification of thematic layers has limited applicability across regions. Furthermore, the highest plausibility resulting from the unweighted index suggests that the several site conditions included, are equally important in influencing the presence of pGDV, at least from a global perspective. Finally, the high agreement of the final map in particular with actual GDV information and field measurements indicates that the selection of thematic layers was appropriate.

For further optimisation, the main goal would be to reduce the

overestimation of pGDV. This could be achieved by subdividing the biome into ecozones, possibly integrating further improved global datasets, and calibrating to more ground data.

The novel map attributes 31 % of the natural vegetation pixels in the Mediterranean with a high potential to be GDV. Highest share occurs in lowlands close to the coast. Those areas indicate precipitation-independent high vitality and evapotranspiration of natural vegetation in low permeable valleys or at low slope areas where water accumulates and the groundwater table is shallow, while soil properties allow infiltration. The results for the Mediterranean can support prioritisation of areas for essential regional high-resolution identification of pGDV.

CRediT authorship contribution statement

Léonard El-Hokayem: Conceptualization, Methodology, Software, Validation, Writing – original draft, Visualization. **Pantaleone De Vita:** Validation, Resources, Writing – review & editing. **Muhammad Usman:** Methodology, Writing – review & editing. **Andreas Link:** Writing – review & editing. **Christopher Conrad:** Conceptualization, Resources, Writing – review & editing, Supervision.

Declaration of competing interest

The authors declare that they have no known competing financial interests or personal relationships that could have appeared to influence the work reported in this paper.

Data availability

Data is uploaded and reviewed at Pangea data publisher (PDI-34769)

Acknowledgement

Funding: The research was funded by the Federal State of Saxony-Anhalt via the MLU|BioDivFund.

We gratefully acknowledges the support of the German Centre for Integrative Biodiversity Research (iDiv) Halle-Jena-Leipzig funded by the German Research Foundation (FZT 118). Special thanks to Patrícia Páscoa for sharing their pGDV map from the Iberian Peninsula and to David Emanuel Schulz for supporting the field campaign.

References

Abijith, D., Saravanan, S., Singh, L., Jennifer, J.J., Saranya, T., Parthasarathy, K., 2020. GIS-based multi-criteria analysis for identification of potential groundwater recharge zones-a case study from Ponnaniyaru watershed, Tamil Nadu, India. HydroResearch 3, 1–14. https://doi.org/10.1016/j.hydres.2020.02.002.

Akasheh, O.Z., Neale, C.M.U., Jayanthi, H., 2008. Detailed mapping of riparian vegetation in the middle Rio Grande River using high-resolution multi-spectral airborne remote sensing. J. Arid Environ. 72, 1734–1744. https://doi.org/10.1016/j.jaridenv.2008.03.014.

Arulbalaji, P., Padmalal, D., Sreelash, K., 2019. GIS and AHP techniques based delineation of groundwater potential zones: a case study from southern Western Ghats, India. Sci. Rep. 9 (1), 1–17. https://doi.org/10.1038/s41598-019-38567-x.

Barbeta, A., Mejía-Chang, M., Ogaya, R., Voltas, J., Dawson, T.E., Penuelas, J., 2015. The combined effects of a long-term experimental drought and an extreme drought on the use of plant-water sources in a Mediterranean forest. Glob. Chang. Biol. 21, 1213–1225. https://doi.org/10.1111/gcb.12785.

Beck, H.E., Zimmermann, N.E., McVicar, T.R., Vergopolan, N., Berg, A., Wood, E.F., 2018. Present and future Köppen-Geiger climate classification maps at 1-km resolution. Sci. Data 5, 180214. https://doi.org/10.1038/sdata.2018.214.

Belgiu, M., Drăguţ, L., 2016. Random forest in remote sensing: a review of applications and future directions. ISPRS J. Photogramm. Remote Sens. 114, 24–31. https://doi.org/10.1016/j.isprsjprs.2016.01.011.

Benz, S.A., Bayer, P., Blum, P., 2017. Global patterns of shallow groundwater temperatures. Environ. Res. Lett. 12, 034005 https://doi.org/10.1088/1748-9326/aa5fb0.

Box, J.B., Leiper, I., Nano, C., Stokeld, D., Jobson, P., Tomlinson, A., Cobban, D., Bond, T., Randall, D., Box, P., 2022. Mapping terrestrial groundwater-dependent ecosystems in arid Australia using Landsat-8 time-series data and singular value decomposition. Remote Sens. Ecol. Conserv. 8 (4), 464–476. https://doi.org/10.1002/rse2.254.

Breiman, L., 1984. Classification and Regression Trees. Routledge, New York. https://doi.org/10.1201/9781315139470.

Breiman, L., 2001. Random Forests. Mach. Learn. 45, 5–32. https://doi.org/10.1023/A:1010933404324.

Buchhorn, M., Lesiv, M., Tsendbazar, N.E., Herold, M., Bertels, L., Smets, B., 2020. Copernicus Global Land Cover Layers-Collection 2. Remote Sensing 2020, 12, 108, 1044. https://doi.org/10.3390/rs12061044.

Canadell, J., Jackson, R.B., Ehleringer, J.R., Mooney, H.A., Sala, O.E., Schulze, E.D., 1996. Maximum rooting depth of vegetation types at the global scale. Oecologia 108 (4), 583–595. https://doi.org/10.1007/BF00329030.

Cohen, J., 1960. A coefficient of agreement for nominal scales. Educ. Psychol. Meas. 20, 37–46. https://doi.org/10.1177/001316446002000104.

Congalton, R.G., 1991. A review of assessing the accuracy of classifications of remotely sensed data. Remote Sens. Environ. 37 (1), 35–46. https://doi.org/10.1016/0034-4257(91)90048-b.

Department of Environment and Science, Queensland, 2013. Plants of potential groundwater dependent ecosystem aquifer mapping extent, Wetland*Info* website. Accessed 11 May 2023, available at: https://wetlandinfo.des.qld.gov.au/wetlands/facts-maps/wildlife/?AreaID=gde-potential-aquifer-extent&Kingdom=plants.

Dhar, A., Sahoo, S., Sahoo, M., 2015. Identification of groundwater potential zones considering water quality aspect. Environ. Earth Sci. 74 (7), 5663–5675. https://doi.org/10.1007/s12665-015-4580-7.

Didan, K., 2015. MOD13Q1 MODIS/Terra Vegetation Indices 16-Day L3 Global 250m SIN Grid V006 [Data set]. NASA EOSDIS Land Processes DAAC. https://doi.org/10.5067/MODIS/MOD13Q1.006.

Doody, T.M., Barron, O.V., Dowsley, K., Emelyanova, I., Fawcett, J., Overton, I.C., Pritchard, J.L., Van Dijk, A., Warren, G., 2017. Continental mapping of groundwater dependent ecosystems: a methodological framework to integrate diverse data and expert opinion. J. Hydrol. Reg. Stud. 10, 61–81. https://doi.org/10.1016/j.ejrh.2017.01.003.

Dorsey, N.E., 1940. Properties of ordinary water-substance in all its phases; water-vapor, water and all the ices. In: Amer. Chem. Soc. Monogr. No. 81, Reinhold, New York. https://doi.org/10.1038/146145a0.

Duran-Llacer, I., Arumí, J.L., Arriagada, L., Aguayo, M., Rojas, O., González-Rodríguez, L., Rodríguez-López, L., Martínez-Retureta, R., Oyarzún, R., Singh, S.K., 2022. A new method to map groundwater-dependent ecosystem zones in semi-arid environments: a case study in Chile. Sci. Total Environ. 816, 151528 https://doi.org/10.1016/j.scitotenv.2021.151528.

Eamus, D., Froend, R., Loomes, R., Hose, G., Murray, B., 2006. A functional methodology for determining the groundwater regime needed to maintain the health of groundwater-dependent vegetation. Aust. J. Bot. 54 (2), 97–114. https://doi.org/10.1071/BT05031.

El-Hokayem, L., De Vita, P., Conrad, C., 2023. Local identification of groundwater dependent vegetation using high-resolution Sentinel-2 data – a Mediterranean case study. Ecol. Indic. 146, 109784 https://doi.org/10.1016/j.ecolind.2022.109784.

Ellenberg, H., 1974. Zeigerwerte der Gefäßpflanzen Mitteleuropas. Scripta Geobotanica 9, 1–97.

Evaristo, J., McDonnell, J., 2017. Prevalence and magnitude of groundwater use by vegetation: a global stable isotope meta-analysis. Sci. Rep. 7, 44110. https://doi.org/10.1038/srep44110.

Fan, Y., Li, H., Miguez-Macho, G., 2013. Global patterns of groundwater table depth. Science 339, 940–943. https://doi.org/10.1126/science.1229881.

Fan, Y., Miguez-Macho, G., Jobbágy, E.G., Jackson, R.B., Otero-Casal, C., 2017. Hydraulic regulation of plant rooting depth. PNAS 114, 40. https://doi.org/10.1073/pnas.1712381114.

Farr, T.G., Rosen, P.A., Caro, E., Crippen, R., Duren, R., Hensley, S., Kobrick, M., Paller, M., Rodriguez, E., Roth, L., Seal, D., Shaffer, S., Shimada, J., Umland, J., Werner, M., Oskin, M., Burbank, D., Alsdorf, D.E., 2007. The shuttle radar topography mission. Rev. Geophys. 45 (2), RG2004 https://doi.org/10.1029/2005RG000183.

Fildes, S.G., Doody, T.M., Bruce, D., Clark, I.F., Batelaan, O., 2023. Mapping groundwater dependent ecosystem potential in a semi-arid environment using a remote sensing-based multiple-lines-of-evidence approach. Int. J. Digital Earth 16 (1), 375–406. https://doi.org/10.1080/17538947.2023.2176557.

Foody, G.M., 2020. Explaining the unsuitability of the kappa coefficient in the assessment and comparison of the accuracy of thematic maps obtained by image classification. Remote Sens. Environ. 239, 111630 https://doi.org/10.1016/j.rse.2019.111630.

Freeze, R.A., Cherry, J.A., 1979. Groundwater. Prentice-Hall, Englewood Cliffs, New Jersey, p. 604.

Funk, C., Peterson, P., Landsfeld, M., Pedreros, D., Verdin, J., Shukla, S., Husak, G., Rowland, J., Harrison, L., Hoell, A., Michaelsen, J., 2015. The climate hazards infrared precipitation with stations—a new environmental record for monitoring extremes. Sci. Data 2, 150066. https://doi.org/10.1038/sdata.2015.66.

Glanville, K., Sheldon, F., Butler, D., Capon, S., 2023. Effects and significance of groundwater for vegetation: a systematic review. Sci. Total Environ. 875, 162577 https://doi.org/10.1016/j.scitotenv.2023.162577.

Goepel, K.D., 2018. Implementation of an Online Software Tool for the Analytic Hierarchy Process (AHP-OS). Int. J. Anal. Hierarchy Process 10 (3), 469–487. https://doi.org/10.13033/ijahp.v10i3.590.

Gomes Marques, I., Nascimento, J., Cardoso, R.M., Miguéns, F., Condesso de Melo, M.T., Soares, P.M.M., Gouveia, C.M., Kurz Besson, C., 2019. Mapping the suitability of groundwater-dependent vegetation in a semi-arid Mediterranean area. Hydrol. Earth Syst. Sci. 23, 3525–3552. https://doi.org/10.5194/hess-23-3525-2019.Gorelick, N., Hancher, M., Dixon, M., Ilyushchenko, S., Thau, D., & Moore, R., 2017. Google Earth

Engine: Planetary-scale geospatial analysis for everyone. Remote Sensing of Environment. 202, 18-27, 10.1016/j.rse.2017.06.031.
Gou, S., Gonzales, S., Miller, G.R., 2015. Mapping potential groundwater-dependent ecosystems for sustainable management. Groundwater 53 (1), 99–110. https://doi.org/10.1111/gwat.12169.
Government of South Australia, 2023. NatureMaps. Accessed 11 May 2023, available at: http://spatialwebapps.environment.sa.gov.au/naturemaps/?locale=en-us&viewer=naturemaps.
Greenberg, J.A., 2021. spatial.tools: R Functions for Working With Spatial Data. R Package Version 1.6.2.
Hartmann, J., Moosdorf, N., 2012. The new global lithological map database GLiM: a representation of rock properties at the Earth surface. Geochem. Geophys. Geosyst. 13, Q12004. https://doi.org/10.1029/2012GC004370.
Hengl, T., 2018. Soil texture classes (USDA system) for 6 soil depths (0, 10, 30, 60, 100 and 200 cm) at 250 m (Version v02) [Data set]. Zenodo. https://doi.org/10.5281/zenodo.1475451.
Hubbert, M.K., 1956. Darcy's law and the field equations of the flow of underground fluids. Trans. Amer. Inst. Min. Met. Eng. 207, 222–239. https://doi.org/10.2118/749-G.
Huscroft, J., Gleeson, T., Hartmann, J., Börker, J., 2018. Compiling and mapping global permeability of the unconsolidated and consolidated Earth: GLobal HYdrogeology MaPS 2.0 (GLHYMPS 2.0). Geophys. Res. Lett. 45, 4. https://doi.org/10.1002/2017GL075860.
Jones, C., Stanton, D., Hamer, N., Denner, S., Singh, K., Flook, S., Dyring, M., 2020. Field investigation of potential terrestrial groundwater-dependent ecosystems within Australia's Great Artesian Basin. Hydrogeol. J. 28, 237–261. https://doi.org/10.1007/s10040-019-02081-1.
Killroy, G., Dunne, F., Ryan, J., O'Connor, Á., Daly, D., Craig, M., Coxon, C., Johnston, P., Moe, H., 2008. A Framework for the Assessment of Groundwater-Dependent Terrestrial Ecosystems under the Water Framework Directive. Environmental Protection Agency, Wexford. Available at. https://www.epa.ie/publications/research/water/erc-report-12.php.
Klausmeyer, K., Howard, J., Keeler-wolf, T., Davis-Fadtke, K., Hull, R., Lyons, A., 2018. Mapping Indicators of Groundwater Dependent Ecosystems in California. California, San Francisco.
Kløve, B., Ala-Aho, P., Bertrand, G., Gurdak, J.J., Kupfersberger, H., Kvaerner, J., Muotka, T., Mykrä, H., Preda, E., Rossi, P., Bertrachi, C., Velasco, E., Pulido-Velazquez, M., 2014. Climate change impacts on groundwater and dependent ecosystems. J. Hydrol. 518, 250–266. https://doi.org/10.1016/j.jhydrol.2013.06.037.
Lehner, B., Grill, G., 2013. Global river hydrography and network routing: baseline data and new approaches to study the world's large river systems. Hydrol. Process. 27 (15), 2171–2186. https://doi.org/10.1002/hyp.9740.
Lewis, J., 2011. The application of Ecohydrological groundwater indicators to hydrogeological conceptual models. Groundwater 50 (5), 679–689. https://doi.org/10.1111/j.1745-6584.2011.00899.x.
Lin, P., Pan, M., Wood, E.F., Yamazaki, D., Allen, G.H., 2021. A new vector-based global river network dataset accounting for variable drainage density. Sci. Data 8, 21. https://doi.org/10.1038/s41597-021-00819-9.
Link, A., El-Hokayem, L., Usman, M., Conrad, C., Reinecke, R., Berger, M., Wada, Y., Coroama, V., Finkbeiner, M., 2023. Groundwater-dependent ecosystems at risk –global hotspot analysis and implications. Environ. Res. Lett. https://doi.org/10.1088/1748-9326/acea97. In press.
Liu, C., Liu, H., Yu, Y., Zhao, W., Zhang, Z., Guo, L., Yetemen, O., 2021. Mapping groundwater-dependent ecosystems in arid Central Asia: implications for controlling regional land degradation. Sci. Total Environ. 797 https://doi.org/10.1016/j.scitotenv.2021.149027.
Magesh, N.S., Chandrasekar, N., Soundranayagam, J.P., 2012. Delineation of groundwater potential zones in Theni district, Tamil Nadu, using remote sensing, GIS and MIF techniques. Geosci. Front. 3, 189–196. https://doi.org/10.1016/j.gsf.2011.10.007.
Martínez-Santos, P., Renard, P., 2020. Mapping groundwater potential through an ensemble of big data methods. Groundwater. 58 (4), 583–597. https://doi.org/10.1111/gwat.12939.
Martínez-Santos, P., Díaz-Alcaide, S., De la Hera-Portillo, A., Gómez-Escalonilla, V., 2021. Mapping groundwater-dependent ecosystems by means of multi-layer supervised classification. J. Hydrol. 603, 126873 https://doi.org/10.1016/j.jhydrol.2021.126873.
Meinzer, O.E., 1927. Plants as indicators of ground water. USGS Water-Suppl. Pap. 577 https://doi.org/10.3133/wsp577.
Mittermeier, R.A., Gil, P.R., Hoffmann, M., Pilgrim, J., Brooks, T., Mittermeier, C.G., Lamoreux, J., Da Fonseca, G.A.B., 2005. Hotspots Revisited: Earth's Biologically Richest and Most Endangered Terrestrial Ecoregions. University of Chicago Press, Conservation International.
Mohan, C., Western, A.W., Wei, Y., Saft, M., 2018. Predicting groundwater recharge for varying land cover and climate conditions–a global meta-study. Hydrol. Earth Syst. Sci. 22 (5), 2689–2703. https://doi.org/10.5194/hess-22-2689-2018.
Mollinedo, J., Schumacher, T.E., Chintala, R., 2015. Influence of feedstocks and pyrolysis on biochar's capacity to modify soil water retention characteristics. J. Anal. Appl. Pyrolysis 114, 100–108. https://doi.org/10.1016/j.jaap.2015.05.006.
Münch, Z., Conrad, J., 2007. Remote sensing and GIS based determination of groundwater dependent ecosystems in the Western cape, South Africa. Hydrogeol. J. 15, 19–28. https://doi.org/10.1007/s10040-006-0125-1.
Murmu, P., Kumar, M., Lal, D., Sonker, I., Singh, S.K., 2019. Delineation of groundwater potential zones using geospatial techniques and analytical hierarchy process in Dumka district, Jharkhand, India. Groundw. Sustain. Dev. 9, 100239 https://doi.org/10.1016/j.gsd.2019.100239.
Nampak, H., Pradhan, B., Abd Manap, M., 2014. Application of GIS based data driven evidential belief function model to predict groundwater potential zonation. J. Hydrol. 513, 283–300. https://doi.org/10.1016/j.jhydrol.2014.02.053.
Pande, C.B., Moharir, K.N., Panneerselvam, B., Singh, S.K., Elbeltagi, A., Pham, Q.B., Varadem, A.M., Rajesh, J., 2021. Delineation of groundwater potential zones for sustainable development and planning using analytical hierarchy process (AHP), and MIF techniques. Appl Water Sci 11, 186. https://doi.org/10.1007/s13201-021-01522-1.
Páscoa, P., Gouveia, C.M., Kurz-Besson, C., 2020. A simple method to identify potential groundwater-dependent vegetation using NDVI MODIS. Forests 11, 147. https://doi.org/10.3390/f11020147.
Pelletier, J.D., Broxton, P.D., Hazenberg, P., Zeng, X., Troch, P.A., Niu, G., Williams, Z.C., Brunke, M.A., Gochis, D., 2016. Global 1-km Gridded Thickness of Soil, Regolith, and Sedimentary Deposit Layers. ORNL DAAC. https://doi.org/10.3334/ORNLDAAC/1304.
Pérez Hoyos, I.C., Krakauer, N.Y., Khanbilvardi, R., Armstrong, R.A., 2016. A review of advances in the identification and characterization of groundwater dependent ecosystems using geospatial technologies. Geosciences 6, 17. https://doi.org/10.3390/geosciences6020017.
Pignatti, S., 2003. The Mediterranean ecosystem. Bocconea 16 (1), 29–40.
Pignatti, S., Menegoni, P., Pietrosanti, S., 2005. Biondicazione attraverso le piante vascolari. Valori di indicazione secondo Ellenberg (Zeigerwerte) per le specie della Flora d'Italia. Braun-Blanquetia 39, 1–97.
Poggio, L., de Sousa, L.M., Batjes, N.H., Heuvelink, G.B.M., Kempen, B., Ribeiro, E., Rossiter, D., 2021. SoilGrids 2.0: producing soil information for the globe with quantified spatial uncertainty. SOIL 7, 217–240. https://doi.org/10.5194/soil-7-217-2021.
Pontius, R.G., Millones, M., 2011. Death to kappa: birth of quantity disagreement and allocation disagreement for accuracy assessment. Int. J. Remote Sens. 32 (15), 4407–4429. https://doi.org/10.1080/01431161.2011.552923.
Rampheri, M.B., Dube, T., Dondofema, F., Dalu, T., 2023. Identification and delineation of groundwater dependent ecosystems (GDEs) in the Khakea–Bray transboundary aquifer region using geospatial techniques. Geocarto Int. 38 (1), 2172217. https://doi.org/10.1080/10106049.2023.2172217.
Rodell, M., Chen, J., Kato, H., Famiglietti, J.S., Nigro, J., Wilson, C.R., 2007. Estimating groundwater storage changes in the Mississippi River basin (USA) using GRACE. Hydrogeol. J. 15 (1), 159–166. https://doi.org/10.1007/s10040-006-0103-7.
Rouse, J.W., Haas, R.H., Schell, J.A., Deering, D.W., Harlan, J.C., 1974. Monitoring the Vernal Advancement of Retrogradation of Natural Vegetation. NASA/GSFC, Type III, Final Report, p. 371.
Running, S., Mu, Q., Zhao, M., 2017. MOD16A3 MODIS/Terra Net Evapotranspiration Yearly L4 Global 500 m SIN Grid (006) [Data set]. NASA EOSDIS Land Processes DAAC. https://doi.org/10.5067/MODIS/MOD16A3.006.
Saaty, T.L., 1986. Axiomatic foundation of the analytic hierarchy process. Manag. Sci. 32, 841–855. https://doi.org/10.1287/mnsc.32.7.841.
Saaty, T.L., 1990. How to make a decision: the analytic hierarchy process. Eur. J. Oper. Res. 48, 9–26. https://doi.org/10.1016/0377-2217(90)90057-I.
Shen, R., Pennell, K.G., Suuberg, E.M., 2013. Influence of soil moisture on soil gas vapor concentration for vapor intrusion. Environ. Eng. Sci. 30 (10), 628–637. https://doi.org/10.1089/ees.2013.0133.
Singh, P., Thakur, J.K., Kumar, S., 2013. Delineating groundwater potential zones in a hard-rock terrain using geospatial tools. Hydrol. Sci. J. 58 (1), 213–223. https://doi.org/10.1080/02626667.2012.745644.
Styron, R., Pagani, M., 2020. The GEM global active faults database. Earthq. Spectra 36 (1), 160–180. https://doi.org/10.1177/8755293020944182.
Sun, J., He, F., Zhang, Z., Shao, H., Pan, Y., Yang, R., Li, W., Li, P., Zheng, M., 2018. Analysis of saline groundwater infiltration into two loam soils. Land Degrad. Dev. 29 (10), 3795–3802. https://doi.org/10.1002/ldr.3089.
Thanh, N.N., Thunyawatcharakul, P., Nguyen, H.N., Chotpantarat, S., 2022. Global review of groundwater potential models in the last decade: parameters, model techniques, and validation. J. Hydrol. 614, 128501 https://doi.org/10.1016/j.jhydrol.2022.128501.
Theobald, D.M., Harrison-Atlas, D., Monahan, W.B., Albano, C.M., 2015. Ecologically-relevant maps of landforms and physiographic diversity for climate adaptation planning. PLoS One 10 (12), e0143619. https://doi.org/10.1371/journal.pone.0143619.
Thomas, F.M., 2014. Ecology of phreatophytes. In: Lüttge, U., et al. (Eds.), Progress in Botany 75. Springer, pp. 335–375.
Tuel, A., Eltahir, E.A.B., 2020. Why is the Mediterranean a climate change hot spot? J. Clim. 33 (14), 5829–5843. https://doi.org/10.1175/JCLI-D-19-0910.1.
Tweed, S.O., Leblanc, M., Webb, J.A., Lubczynski, M.W., 2007. Remote sensing and GIS for mapping groundwater recharge and discharge areas in salinity prone catchments, southeastern Australia. Hydrogeol. J. 15 (1), 75–96. https://doi.org/10.1007/s10040-006-0129-x.
Underwood, E.C., Viers, J.H., Klausmeyer, K.R., Cox, R.L., Shaw, M.R., 2009. Threats and biodiversity in the Mediterranean biome. Divers. Distrib. 15, 188–197. https://doi.org/10.1111/j.1472-4642.2008.00518.x.
Weast, R.C., 1987. Handbook of Chemistry and Physics, 68th ed. CRC Press, Cleveland, Ohio.
Yamazaki, D., Ikeshima, D., Sosa, J., Bates, P.D., Allen, G.H., Oavelsky, T.M., 2019. MERIT hydro: a high-resolution global hydrography map based on latest topography dataset. Water Resour. Res. 55, 5053–5073. https://doi.org/10.1029/2019WR024873.